NTNU
Norwegian University of
Science and Technology

Influence of Cracks on Chloride Ingress and Reinforcement Corrosion

Andreas Rygg

Civil and Environmental Engineering
Submission date: June 2017
Supervisor: Mette Rica Geiker, KT
Co-supervisor: Tobias Alexander Danner, KT

Norwegian University of Science and Technology
Department of Structural Engineering

Department of Structural Engineering
Faculty of Engineering Science and Technology
NTNU- Norwegian University of Science and Technology

ACCESSIBILITY

Open

MASTER THESIS 2017

SUBJECT AREA:	DATE:	NO. OF PAGES:
Concrete Technology	11.06.2017	46 + 24

TITLE:

Influence of Cracks on Chloride Ingress and Reinforcement Corrosion

Innflytelsen av riss på inntrengning av klorider og armeringskorrosjon

BY:

Andreas Rygg

SUMMARY:
This study focuses on gathering more long-term data on the relation between cracks, chloride ingress and initiating of reinforcement corrosion.

Two bridges in Trondheim were investigated, Moholt Bridge and Cecilie Bridge. Moholt Bridge was half-cell potential mapped. Three cores were drilled from the bridge. One core with 0.55 mm crack width, one with 0.15 mm crack width and one reference core with no crack, all of them included reinforcement. One core was drilled from Cecilie Bridge. This core had a crack width of 0.45 mm and no reinforcement. They were chloride mapped using μ-XRF. Characterization of carbonation was done and the reinforcement was excavated and investigated.

The cores from Moholt Bridge all showed a similar chloride ingress, evenly distanced from the top surface and no additional chloride ingress around the crack and from the crack surface. The core from Cecilie Bridge showed a chloride ingress both from the top surface and from the crack surface. Both bridges are quite similar constructions, but interestingly they showed opposite results on chloride ingress through cracks.

Corrosion was detected only at the reinforcement closest to the crack in the core from Moholt Bridge, that had a wide crack (0.55 mm). There was not detected any chlorides in the crack, but the crack surface and parts of the concrete area around the reinforcement, was completely carbonated. This could indicate carbonation as the cause of the observed corrosion. The crack surface in the core from Cecilie Bridge was also carbonated.

RESPONSIBLE TEACHER: Mette Rika Geiker

SUPERVISORS: Mette Rika Geiker and Tobias Alexander Danner

CARRIED OUT AT: Department of Structural Engineering, NTNU

Preface

This master's thesis was written by Andreas Rygg at the Norwegian University of Science and Technology (NTNU), Department of Structural Engineering. The work of producing this thesis was performed from January to June 2017 (20 weeks). Mette Rika Geiker was the main supervisor for this thesis.

Through the work of this thesis, I have gained a broader understanding of the problematics on chloride ingress in concrete and how it connects to initiating of reinforcement corrosion. The field work was performed on Moholt Bridge and Cecilie Bridge, both located in Trondheim. Thanks to Ove Loraas for assistance in field work and for drilling the concrete cores. The laboratory work associated with this thesis was done at the NTNU Concrete Research Facility. Thanks to Tobias Danner for helping with the μ-XRF analyses of the cores. Thanks to Tobias Danner and Mette Geiker for writing the draft note on "Carbonation of concrete cores from Moholt- and Ceciliebridge" so that investigation on carbonation could be included in this thesis, despite limited time available.

Trondheim, June 2017

Andreas Rygg

Abstract

Chloride induced reinforcement corrosion is a major durability problem in concrete constructions. It is consensus in literature that cracks facilitate chloride ingress, and may initiate early reinforcement corrosion. This study focuses on gathering more long-term data on the relation between cracks, chloride ingress and initiating of reinforcement corrosion.

Two bridges in Trondheim were investigated, Moholt Bridge and Cecilie Bridge. Moholt Bridge was half-cell potential mapped. Three cores were drilled from the bridge. One core with 0.55 mm crack width, one with 0.15 mm crack width and one reference core with no crack, all of them included reinforcement. One core was drilled from Cecilie Bridge. This core had a crack width of 0.45 mm and no reinforcement. They were chloride mapped using µ-XRF. Characterization of carbonation was done and the reinforcement was excavated and investigated.

The results from the half-cell potential mapping on Moholt Bridge showed a low probability of reinforcement corrosion due to chlorides.

The cores from Moholt Bridge all showed a similar chloride ingress, evenly distanced from the top surface and no additional chloride ingress around the crack and from the crack surface. The core from Cecilie Bridge showed a chloride ingress both from the top surface and from the crack surface. Both bridges are quite similar constructions, but interestingly they showed opposite results on chloride ingress through cracks.

Reinforcement corrosion was only detected in the core with crack width of 0.55 mm from Moholt Bridge. It was located on the reinforcement closest to the crack. There was not detected any chlorides in the crack, but the crack surface and parts of the concrete area around the reinforcement, was completely carbonated. This could indicate carbonation as the cause of the observed corrosion. The crack surface in the core from Cecilie Bridge was also carbonated, but there was no reinforcement to investigate in this core.

Sammendrag

Korrosjon i armering på grunn av klorider, er et stort bestandighetsproblem i konstruksjoner av betong. Det er enighet i litteraturen om at riss legger til rette for inntrengning av klorider og kan initiere tidlig korrosjon i armering. Denne studien fokuser på å innhente mer langtidsdata om relasjonen mellom riss, inntrengning av klorider og initiering av korrosjon i armeringen.

Moholtbrua og Ceciliebrua i Trondheim ble undersøkt. På Moholtbrua ble halvcellepotensialet kartlagt og tre kjerner ble boret fra broen. En kjerne med rissvidde 0,55 mm, en med rissvidde 0,15 mm og en referansekjerne uten noe riss. Det var armering i alle kjernene. En kjerne ble boret fra Ceciliebrua. Denne kjernen hadde et riss på 0,45 mm, men ingen armering. Kloridinnholdet i kjernene ble kartlagt med μ-XRF. Det ble også gjort kartlegging av karbonisering, og armeringen ble gravd frem og undersøkt.

Resultatene fra kartleggingen av halvcellepotensialet på Moholtbrua, viste lav sannsynlighet for at der var korrosjon i armeringen på grunn av klorider.

Kjernene fra Moholtbrua viste alle samme kloridinntrengning, nemlig en jamn fordeling fra den utvendige overflaten og ikke noe større kloridinntrengning rundt og på overflaten til rissene. Kjerne fra Ceciliebrua viste klorid inntrengning både fra den utvendige overflaten og fra overflaten til rissene. De to broene er ganske like konstruksjoner, men interessant nok viste de ulike resultater om kloridinntrengning gjennom riss.

Korrosjon i armeringen ble bare oppdaget i kjernen med 0.55 mm rissvidde fra Moholtbrua, i armeringen nærmest risset. Det var ikke oppdaget klorider i risset, men rissoverflaten og deler av betongoverflaten rundt rissene var fullstendig karbonisert. Dette kan indikere at karbonisering er grunnen til korrosjonen som ble oppdaget. Rissoverflaten til kjernen fra Ceciliebrua var også karbonisert, men det var ingen armering å undersøke i denne kjernen.

Table of contents

List of Abbreviations:

w/c = water/cement ratio

μ-XRF = Micro X-Ray Fluorescence

NPRA = Norwegian Public Roads Administration

ASR = Alkali-Silica Reaction

HCP = Half-Cell Potential

1. Introduction

Chloride induced reinforcement corrosion is a major durability problem in concrete constructions. In principle steel reinforcement embedded in concrete is the perfect match. Steel provides the tensile strength that concrete lack, and concrete cover protect the steel. Due to high alkalinity of the concrete pore solution, a protective passive layer is formed around the steel reinforcement. Chloride that penetrate the concrete and reach the reinforcement, breaks down this passive layer. This will initiate destructive corrosion. (Pease 2010, Geiker 2012)

Cracks are an inherent part of reinforced concrete. They form because of low tensile strain capacity of concrete. Several common mechanisms could be responsible that concrete exceed this capacity. It is consensus in literature that cracks facilitate chloride ingress, and may initiate early reinforcement corrosion. There is an interest in gathering more longterm data on the relation between cracks and chloride ingress. (Hornbostel and Geiker 2016) For example what is now considered a harmful crack width in the Eurocode, 0.3 mm or higher, is an assumption (Beeby 1978). And it must be, until there exists improved understanding and sufficient supporting field data.

Long-term data on the influence of cracks on chloride ingress and reinforcement corrosion are lacking. Some field surveys (Lindquist et al. 2006) have obtained long-term data, but most of the research are experiments done in the laboratory (Michel et al. 2013). Ability to control each different factor, for example exposure, crack width etc. is an advantage in a laboratory experiment. But there are combinations and variations naturally happening in a construction during a lengthy period. And that information is needed to apply the lab results in real life. Doing field studies on structures gives the opportunity to consider these long-term effects that likely have influenced the observed chloride ingress and reinforcement corrosion. That could be different crack types, including time of development, expected variations of crack width and perhaps self healing of the cracks. Or variation in exposure, loading, weather conditions etc. The limitations of a field study are the uncertainty in these attributes. (Hornbostel and Geiker 2016)

The ability to use the new μ-XRF to analyze chloride ingress in cores from bridges, are a helpful tool. In another bridge investigation from Kansas, (Lindquist et al. 2006) they had to grind the concrete to analyze the chloride content. Both slow and destructive compared to the μ-XRF, which uses X-rays and don't spoil the sample (Danner et al. 2017).

1.1. Objectives

The objectives of this project are as listed below:

- Examine the impact of cracks on chloride ingress in field exposed structures.
- Examine the impact of cracks on reinforcement corrosion in field exposed structures.

1.2. Method and limitations

This project focus on collecting long term field data on crack widths impact on chloride ingress and corrosion. The edge beam adjacent to the pedestrian lane on two bridges in Trondheim, Moholt Bridge and Cecilie Bridge, were investigated. During the Norwegian

winter, they are exposed to de-icing salt, although exact information on use of de-icing salt were not achievable.

Moholt Bridge was first visually inspected. Crack width were compared to an earlier student investigation (Skare and Stemland 2015) and close of pictures were taken along the whole edge beam. Then half-cell potential mapping of the reinforcement was done.

In correlation to that, resistivity of the concrete and cover depth to the reinforcement were measured. Then, at points of interest, concrete cores were drilled and examined further in the laboratory. Cores were drilled at locations with large crack width (0.55mm), small crack width (0.15 mm) and no crack. All cores contained reinforcement. In the laboratory, the cores were sawed in half. Then µ-XRF was used on one half to map the elements in the core, with focus on the amount and distribution of chloride. Some of the other core halves were tested for carbonation with thymolphthalein and the reinforcement were excavated and inspected.

Cecile Bridge was inspected when the field work on Moholt Bridge were done. Crack width for part of that bridge were also included in the student report (Skare and Stemland 2015). A core was drilled on a wide crack (0.45 mm) in the edge beam of Cecile Bridge. No reinforcement was included in this core. Amount of chloride was checked in the µ-XRF. Thymolphthalein was sprayed in the crack to check carbonation. These results were also used to get an indication on the value of further and more detailed investigations on the bridge.

2. Theory

2.1. Chloride ingress and reinforcement corrosion

The critical chloride content, C_{crit}, that breaks down the protective passive layer around a reinforcement embedded in concrete, are given in Table 2.1. These values are still in discussion. They depend on the test method and an accepted and standardized test method does not yet exist. (Angst et al. 2009)

Table 2.1 Critical chloride content (Poulsen et al. 1985)

Chloride content [weight % of cement]	Probability of corrosion
< 0.4	Negligible
0.4 – 1.0	Possible
1.0 – 2.0	Likely
> 2.0	Certain

Chloride will enter the concrete, either as dissolved in water by capillary suction or permeation, or by diffusion through the pore liquid. A sufficient wide crack so that water penetrate, would have the potential to bring chloride deeper inside the concrete.

In a laboratory study, specimens were exposed to water on the top surface. Results showed that moisture reached greater depths immediately after exposure, when the tested specimens had crack width of 0.1 mm and 0.2 mm. It was indicated that moisture proceeded

rapidly through cracks and that a portion of the crack behaved as free surfaces for water sorption and chloride ion ingress. In terms of diffusion, the ingress of chloride ions is delayed compared to the moisture ingress behavior. (Pease 2010)

A deeper chloride ingress is expected around a crack. An example of that from a laboratory experiment is provided in Figure 2.1. (Michel at el 2013) This was also shown in another study on crack widths influence on penetration depth of chlorides. Crack geometry have an influence too. Parallel cracks cause greater permeability than V-shaped cracks. In that study, the cracks were made using Brazilian splitting test. The results from that study is shown in (Figure 2.2). (Audenaert et al. 2009)

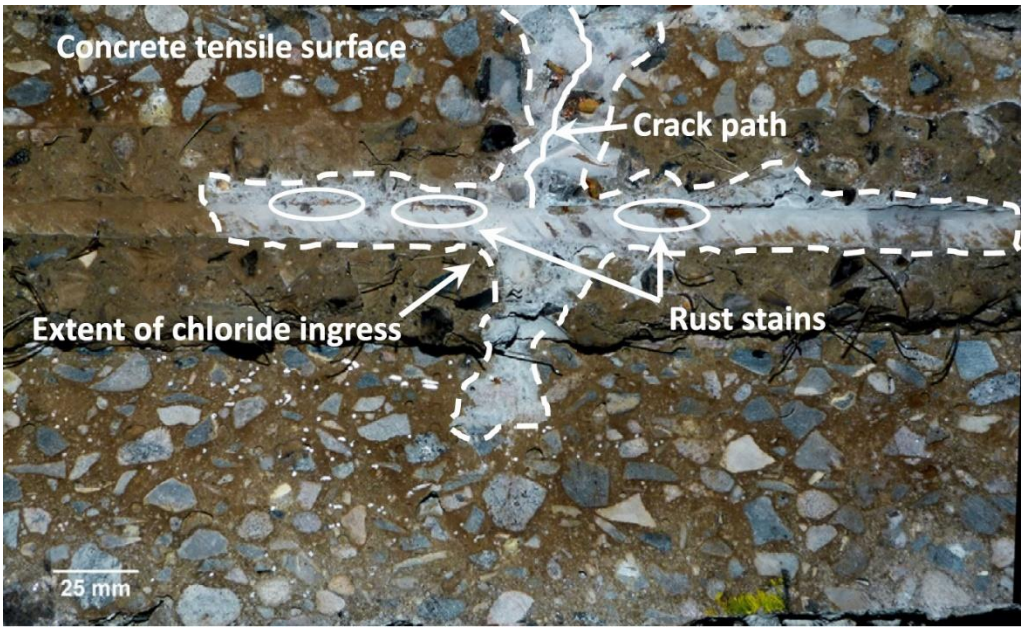

Figure 2.1 Extent of chloride ingress (broken line), crack path (solid line) and rust stains (circled areas) from a laboratory investigation. (Michel et al. 2013)

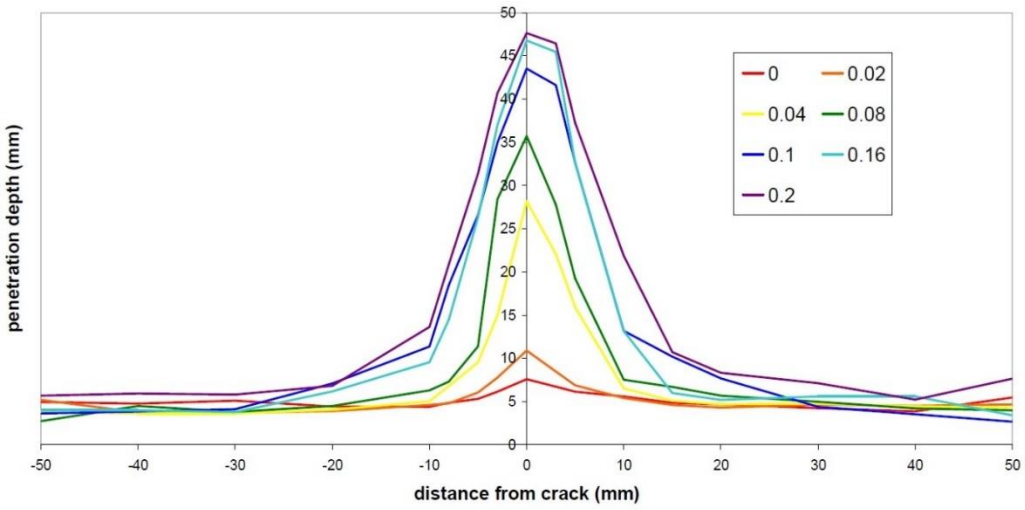

Figure 2.2 Chloride penetration depth for varying crack widths. Cracks were made using Brazilian splitting test. (Audenaert et al. 2009)

Chloride concentration, due to diffusion in an uncracked, homogeneous concrete, at depth (x) after time (t), can be predicted by the error function solution to Fick's 2nd law (Geiker 2012):

$$c(x,t) = c_s - (c_s - c_0)\mathrm{erf}\left(\frac{x}{2\sqrt{D(x,t)\times t}}\right)$$

Self healing of cracks is possible, and this is expected to reduce chloride ingress in cracks. The cement paste could swell near the crack surface, so that the expansion closes the crack. Hydration of unhydrated cement particles, growth of crystal and formation of calcium carbonate on the crack face, are chemical processes that could contribute to self healing. Small particles could also close a crack. (Savija and Schlangen 2016) Variation in loading, as would be expected on a bridge, would potential reopen a self healed crack. And the positive effect of less corrosion due to self healing is then lost. (Otieno et al. 2010)

2.2. Corrosion mechanism for steel embedded in concrete

Reinforcement in concrete is protected by a passive layer. This layers form around the reinforcement because of the high alkalinity (pH from 11 to 14) of the pore solution in concrete. This layer consists of a thin and dense layer of corrosion products on the steel surface, and is preventing further corrosion. However, the passive layer can be destroyed by different mechanisms, resulting in steel corrosion. Carbonation, which is penetration of CO_2 from the exterior, will lower the pH in the concrete. When the pH gets down to around 9, the passive layer become unstable. The passive layers could also be destroyed by presence of chloride ions. Chloride ions commonly originate from seawater or de-icing salt. Where the passive layer is broken, an anode dissolves the steel and rust is formed. Usually the passive steel around the anode act as a cathode. Furthermore, for corrosion to take place there must be access to oxygen (O_2), and moisture. (Pease 2010, Geiker 2012) This is illustrated in Figure 2.3.

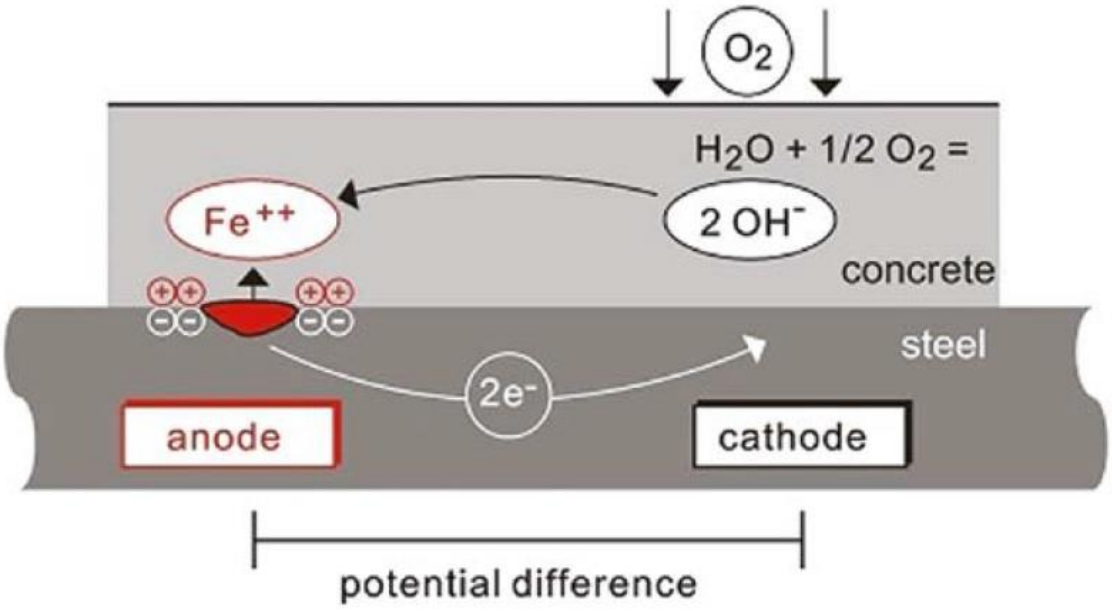

Figure 2.3 Principle of reinforcement corrosion with availability of oxygen. (Proceq SA 2016)

2.3. Electro chemical potential of reinforcement

Risk of corrosion for structures exposed by chlorides from de-icing salts are given in Table 2.2, this is the threshold suggested by Appendix X1 (ASTM 876-15 2015). If the reason for corrosion is carbonation, half-cell potential is generally higher than the half-cell potentials due to chloride induced corrosion. (Geiker and Michel 2017)

Table 2.2 Suggested threshold for half-cell potential measurements (ASTM 876-15 2015)

Half-cell potential [mV CSE]	Probability of corrosion
> 0 mV	None
0 mV - - 200 mV	< 10 %
- 200 mV - - 350 mV	10 % - 90 %
< - 350 mV	> 90 %

Electro chemical potential measurements are based on the difference in electrochemical potential between active (corroding) and passive steel (Geiker and Michel 2017). A potential mapping is done by measuring the electro chemical potential over the whole area of a structure. The aim is to located areas with corroding reinforcement. (Elsener and Bohni 1990) This is useful when deciding where to examine closer. The method used is called half-cell potential measurements and the principle is shown in Figure 2.4. Here the potential difference between the reference electrode as on half-cell and the rebar with concrete cover as the other half-cell is measured. An electrical connection needs to be established between the reinforcement and the reference cell. There are some factors that influence the results from half-cell potential mapping, and therefore they should be measured as well. (Elsener et al. 2003)

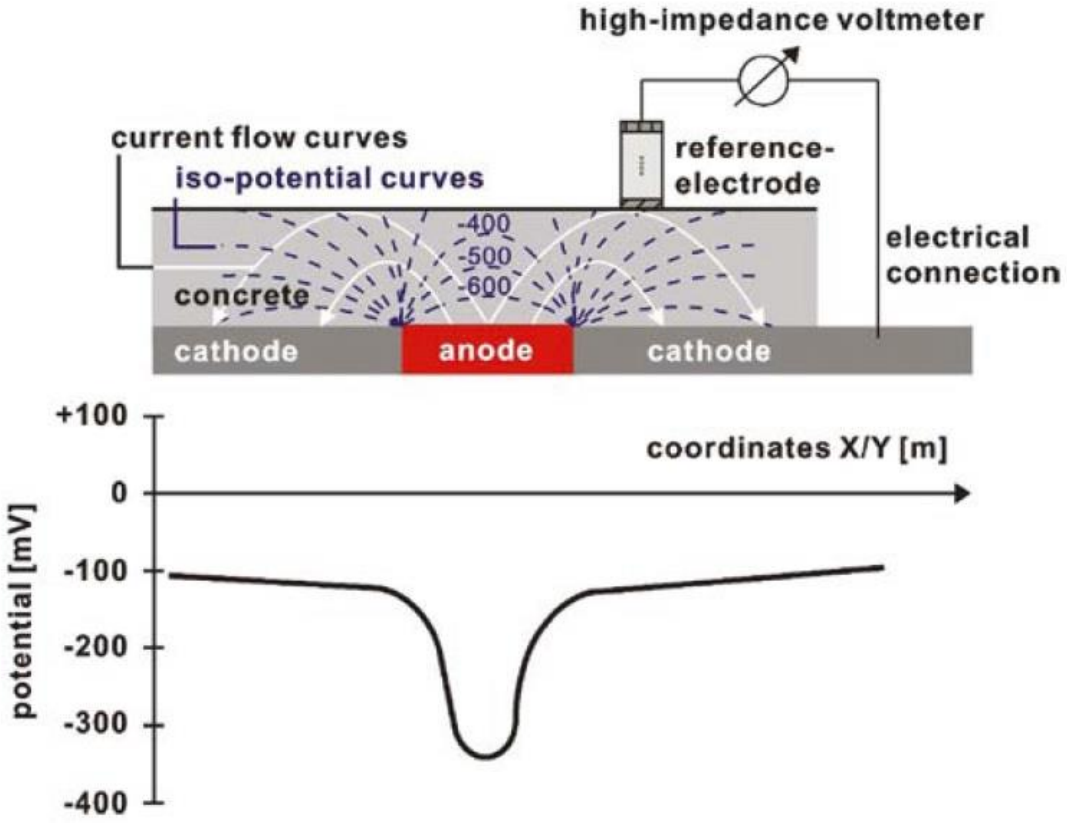

Figure 2.4 Principe of half-cell potential measurements. (Proceq SA 2016)

Resistivity is one factor that influences the results from a half cell potential mapping. Chloride contamination and moister concrete, lowers the resistivity in concrete. It is easier to detect corroding reinforcement in wet concrete. In a high resistivity concrete, pitting corrosion may be difficult to detect. Therefore, care should be taken in choosing a small enough grid width when performing half-cell potential (HCP) measurements. Concrete could be so dry that rusted reinforcement is not detected. (Elsener et al. 2003) In a study a change in resistivity from 22 Ωm to 27 Ωm changed the potential from -600 mV to -530 mV (Elsener and Bohni 1997). The dimension of the values is not directly applicable, there are many factors to consider, but it shows the relation between half-cell potential and resistivity.

The cover depth will also influence the half-cell potential values you measure on the concrete surface. The potential is lowest at the corrosion spot on the reinforcement (anode). It then increases with decreasing distance to the concrete surface. On the concrete surface, it is lowest right on top of the anode. (Elsener et al. 2003)

Analyzing half-cell potential, resistivity and cover depth together must be done to get a good understanding of the results from a half-cell potential mapping. An example is when the measurements of cover depth and resistivity is constant, but the half-cell potential is changing between two different places. That difference in half-cell potential while the other factors are constant, indicates two different corrosion states. Then in another example cover depth, resistivity and half-cell potential all varies between two measured places, it is then not certain that the corrosion states are different. It could be different corrosion states, but it could also be that change in resistivity or cover depth influenced the half-cell potential

measurement, while reality was that the half-cell potential at the reinforcement was the same.

2.4. Resistivity of concrete

Concrete resistivity is a measure of the concrete's ability to transport ions. High resistivity means slow transport, which is good in terms of corrosion. Then the transport of ions between the anode and the cathode, is slower. That slows the corrosion rate (typically given as electrical current density). However, other factors also affect the corrosion and there is no unique correlation between the concrete resistivity and the corrosion rate. For a given concrete resistivity the corrosion rate can vary considerably (Figure 2.5). (Hornbostel et al. 2013)

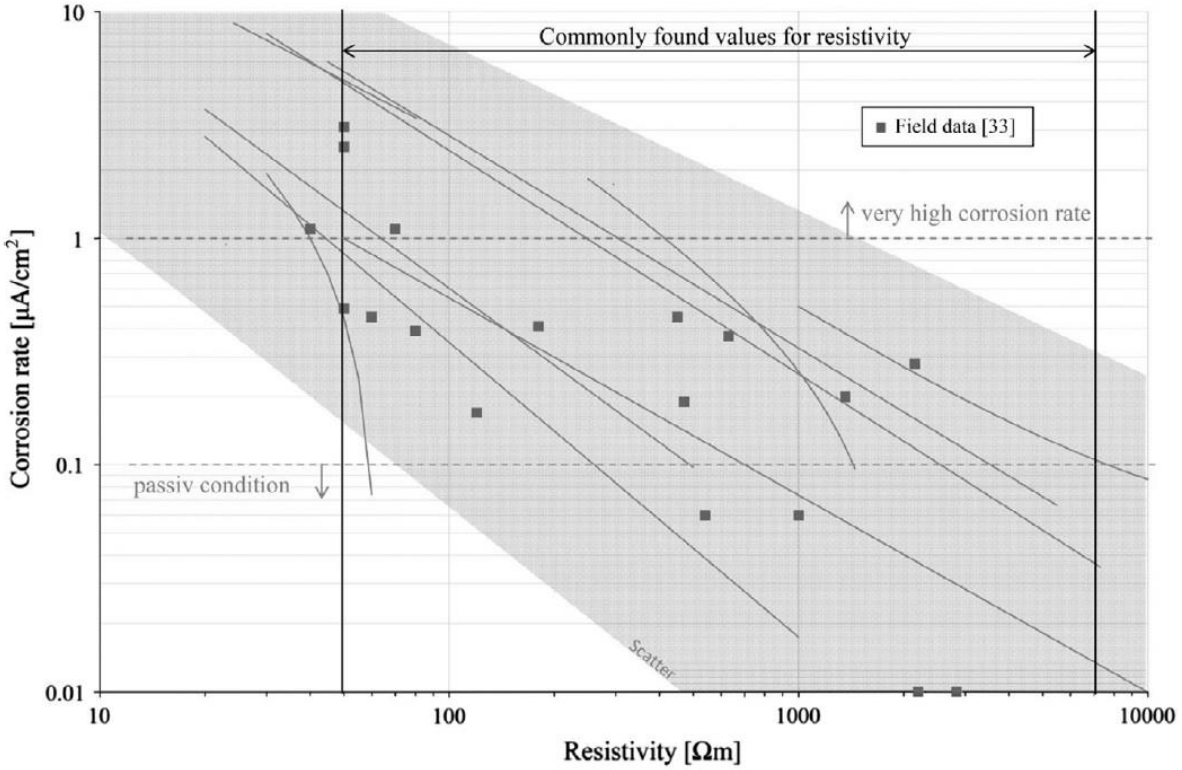

Figure 2.5 A graph on what corrosion rate to expect from different resistivity values. (Hornbostel et al. 2013)

With resistivity measurements alone it is not possible to find out if the reinforcement is actively corroding. Half-cell potential mapping on the other hand can give that information. If the half-cell potential mapping shows that reinforcement is not in an active corroding state, a high risk of corrosion indicated by resistivity is not interesting, since it's already established that there is no ongoing corrosion. In the case of an active corroding steel, a resistivity measurement may show where on a structure the corrosion is strongest (Polder et al. 2000). Values for corrosion risk, dependent of concrete resistivity are given in Table 2.3. This is for temperature 20°C. Empirical studies show that one degree increase in

temperature could reduce the resistivity by 3 % for saturated concrete and 5 % for dry concrete. (Polder et al. 2000)

Table 2.3 Risk of corrosion of reinforcement associated with concrete resistivity for 20°C and OPC concrete. (Polder et al. 2000)

Concrete resistivity $\rho_{concrete}$ ($k\Omega cm$)	Risk of corrosion
< 10	High
10 – 50	Moderate
50 – 100	Low
> 100	Negligible

2.5. Reasons for cracks

Concrete has low tensile strain capacity, approximately 0.01 %. Volume changes would often be higher than that. There is usually some restraint too, which leads to tensile stresses that could exceeds the strain capacity, then cracking occurs. There are several cracking mechanisms and it should also be considered that multiple mechanisms could act simultaneously to cause cracking. One mechanism can start developing a crack at a certain age and another mechanism could amplify or retract the crack. Then the history of the crack development could indicate the type of crack. (Bjontegaard 2009) Considering the time when cracking occurred can give valuable information on how long the crack was open and if variations in crack width during time have happened. A more in detail description of cracks is given in Appendix D.

2.6. Chemical imaging by μ-XRF

μ-XRF (X-Ray Fluorescence) is a chemical imaging technique. An X-ray source excites the atoms in the sample by ionizing electrons from an inner energy level (e.g K-shell) of the atom. An electron from the lower energy level (e.g. L-shell) rapidly refills this inner energy level. The energy difference between the two energy levels is emitted as an X-ray and characteristic for each element. (M4 Tornado manual) μ-XRF can for example be used to study chloride ingress in concrete (Moradllo et al. 2017 and Danner et al. 2017).

3. Structures

3.1. Table of properties

Table 3.1 summarize the properties of the investigated bridges.

Table 3.1 Properties table on investigated bridges

Bridge/Structure	**Cecilie Bridge**	**Moholt Bridge**
Type of structure	Beam bridge	Slab bridge
Geometry	123.9 m long 9.7 m – 11.5 m wide	46.5 m long 21.0 m wide
Location	Trondheim, St. Olavs Hospital	Trondheim, Moholt
Buildingyear	2001	1992
Age (years)	16	25
Exposure	Deicing salt	Deicing salt
Distance to road	2.4 m - 4.2 m	4.0 m
Climate	Inland	Inland
Concrete	C55, SV-40, Armering B500C	C45, m ≤ 0.4, Luft = 5 ± 1.5 % Armering K500TS
Cover	55 mm	50 mm
Type and location of cracks	**Abutment:** Crack with carbonate precipitation **Column**: Map cracking **Edge beam:** Cracks due to shrinkage and external restraint	**Abutment**: Vertical crack in walls **Column (Main girder**): Shear cracks **Edge beam:** Cracks due to shrinkage, external restraint, ASR
Earlier Investigations	Crack documentation (50 m of the bridge)	Crack documentation First inspection by NTNU
Estimated chloride ingress	Unknown	Unknown

3.2. Moholt Bridge

The bridge is in Trondheim, Norway. It's on the road Jonsvannsveien, FV 861, and it's located at Moholt. The bridge spans over the by-pass road, E6 (Omkjøringsveien). It started its service life in 1992. Pictures of the bridge in Figure 3.1 and 3.2.

Figure 3.1 Moholt Bridge seen from the east

Figure 3.2 Moholt Bridge seen from the side

3.2.1. Geometry

The bridge is constructed as a slab bridge. The overall length is 46.5 meters, the two longest spans are 15 meters. It's 21.0 m wide to support four driving lanes and one pedestrian lane. The bridge is slightly curved were the inner radius is 281.8 m and the outer radius is 302.2 m. This present investigation focus on the outer edge beam which neighbors the pedestrian lane. The flat, exposed area of the edge beam is 390 mm wide with a fence located almost in the middle. And the exposed side rises (200mm) above the walking path. Drawings of the bridge is provided in the Appendix A.

3.2.2. Materials

- Concrete class C45
- Environmental class MA
- Air voids 5% ± 1.5 %
- D_{max} = 16 mm
- Reinforcement K500TS

3.2.3. Earlier investigations

There has been an inspection of the edge beam prior to this by NTNU. A potential rust spot on the edge beams surface was located during that inspection. It was probably at 40.20 m in this projects axis system. However, it was unclear if the rust originated from the fence above or from the reinforcement in the concrete. (Hornbostel 2016)

Mapping the crack width was done during the summer of 2015. Only the singular cracks were measured and mapped. (Skare and Stemland 2015)

The NPRA has a digital online database containing information on bridges (BRUTUS). Reports from their own inspections were available as well as the construction drawings were available there.

3.2.4. Exposure to chloride

Driving lanes on Moholt Bridge are regulated as winter maintenance class “DkB” (Vegvesen c 2017), meaning that snow and ice should be removed immediately and salt can be used both preventative and for removal. That indicates high use of salt. The class DkB is the second highest priority for snow removal on Norwegian roads. (Vegvesen a 2017) Data for winter operation before 2015 is not obtained. The direct exposure on the pedestrian lanes is more unclear. The road authorities started using salt on some pedestrian lanes in Trondheim from 2015. Before that there was no use of salt (Minnoreti 2017). This potentially includes Moholt Bridge. From 2015 to 2020 the pedestrian lane on Moholt Bridge is regulated as winter maintenance class “GsB” (Vegvesen b 2017), meaning mechanical removal of snow and use of sand to get wanted friction on snow/ice.

The pedestrian path has a width of 4.0 m, meaning that the investigated edge beam is 4.0 m away from the driving lanes where deicing salts are regularly used in winter maintenance. Furthermore, the bridge has a downslope away from the northern edge beam. On the pedestrian lane, the slope is 3 % and it is 4 % on the driving lanes. Further details of the construction can be seen in the bridge drawings in Appendix A. The weather station at Voll, which is close to the bridge, has statistics of wind direction. Figure 3.3 shows that the main wind direction during winter (November to April 1992-2006) was from south west. (eklima 2017) This is the direction that will hit the bridge perpendicular one the south side (Figure 3.4) and potentially facilitate transport of chloride from de-icing salt to the northern edge beam.

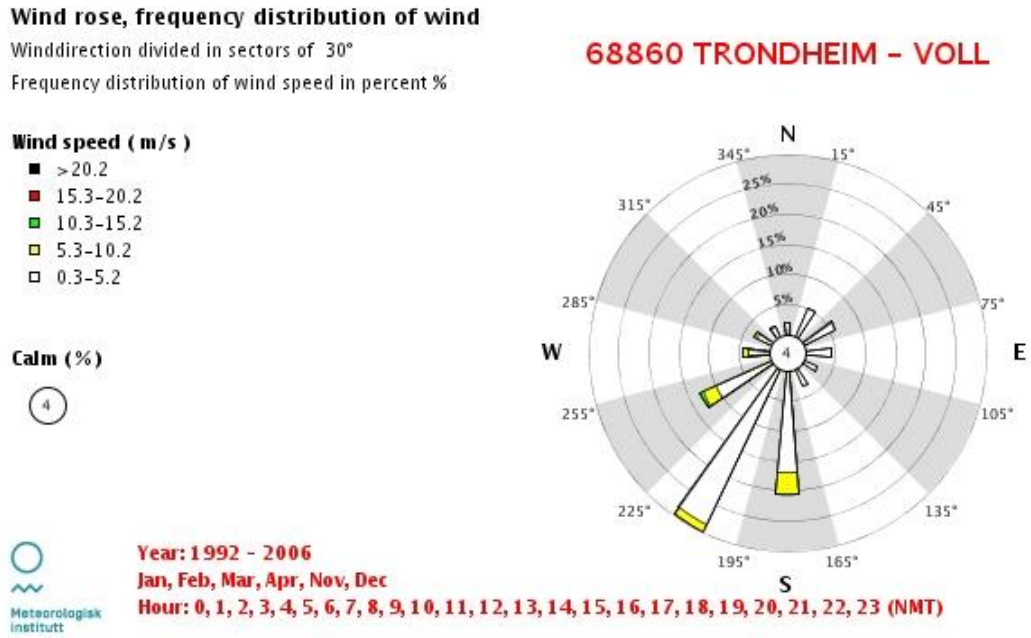

Figure 3.3 Wind rose of the historical measurementeted of wind direction during the winter (1992-2006), at Voll meterological station, which is right by Moholt Bridge. (eklima 2017)

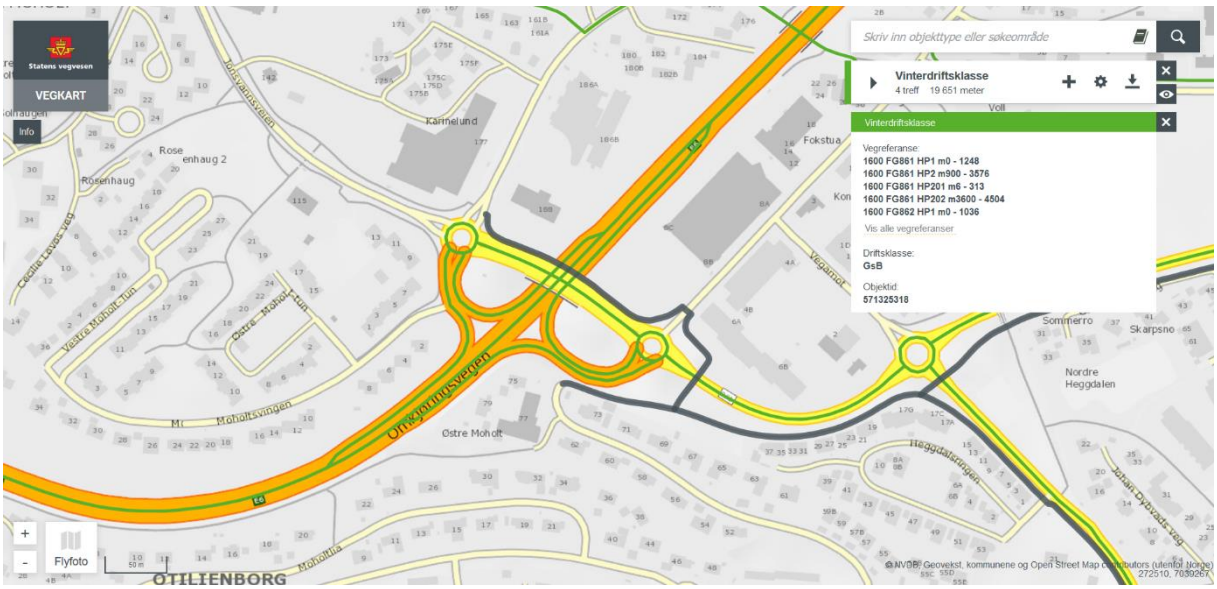

Figure 3.4 Screenshot from NPRA maintenance map on the internet. (Vegvesen b 2017) The bridge is located between the two roundabouts in the center. The marked grey line is the pedestrian line, and we can see the maintenaince regulation is GsB.

The day concrete cores were drilled, a layer of ice was observed on the edge beam. With increasing temperatures during the day, the ice started to melt. Because of the slope on the bride, most places the water drained off the concrete surface. This might indicate that the time chlorides dissolved in water are in direct contact with the concrete surface, is short. Especially if it must penetrate a layer of ice first, giving time for water and chloride to drain off before exposing the concrete surface.

3.2.5. Visual mapping

Investigation showed that the northern edge beam is cracked (Figure 4.2). There is an almost continuous crack pattern on the top surface. It would be described as a map crack pattern where the distance between cracks is approximately 10-20 cm, and they are mostly connected to each other.

There are also singular cracks, that are continuous through the side and the top of the edge beam. On the top surface, they usually coincide with the irregular map pattern cracks. These cracks were already documented in summer 2015 (Skare and Stemland 2015). A distribution of 3-4 cracks per meter was documented in this report. Own investigation in February 2017, was in average one crack every meter. Only cracks observed both on the side and the top surface of the edge beam were considered this time. The cracks were not evenly distributed along the bridge, for example the distribution was more intense above the supports. The crack width varied from 0.1 to 0.6 mm. The singular cracks were assumed to be deep since they were visible both on the top surface and far down the sides.

3.2.6. Repair, maintenance

It was discovered what seem to be extra concrete, added later than the original casting, around the fence posts. An example of that in Figure 3.5.

Figure 3.5 Fence post on Moholt bridge, extra concrete seem to be added around the post.

3.3. Cecilie Bridge

Cecilie Bridge is located between St. Olavs hospital and the area Marienborg, in Trondheim. It spans across the river Nidelva. The bridge started its service life in 2001. Pictures of Cecilie Bridge in Figure 3.6 and 3.7.

Figure 3.6 A overweiv of Cecilie Bridge. Note the curved outer edge next to the pedestrian lane.

3.3.1. Geometry

Cecilie Bridge is a beam bridge approximately 124 meters long. The width varies between 9.725 m and 11.525 m due to a curved edge of the pedestrian lane. The bridge beam is made of steel and the slab is casted in concrete (Figure 3.7).

Figure 3.7 The underside of Cecilie Bridge with the steel beam and connection to the concrete slab.

3.3.2. Materials

- Concrete class C55 SV-40
- Environmental class MA
- Reinforcement K500TE

3.3.3. Earlier investigations

Mapping the crack width was done during the summer of 2015. But only one area on the east side, and on area in the middle of the bridge were mapped. In total 50 meters of the 124 meters long bridge were mapped. (Skare and Stemland 2015)

The bridge has a digital folder with various information in the NPRA online bridge database (BRUTUS). Construction drawings were available there. Information obtained showed that the cover depth to structural reinforcement was projected to be 55 mm. According to the drawings the edge beam was surface treated (probably impregnated) to limit chloride ingress.

3.3.4. Exposure to chloride

Cecilie Bridge is on a communal road, so the NPRA map on winter maintenance don't include it. The exposure on the driving lane is not known. The only information available at the present time is that the pedestrian lane is not one of the priority bicycle paths that are salted as part of the environmental package. (Environmental package 2017)

3.3.5. Visual mapping

There were singular cracks with variable distance, visible both on the side and the top surface of the investigated northern edge beam. Some of them were mapped by Skare and Stemland (2015).

3.3.6. Half-cell potential mapping

Potential mapping was not done at Cecilie Bridge. The drawings show that there is a coating on the edge beam. It is not possible to make a potential measurement through an electrically isolating coating, but it is possible to make a measurement through a thin dispersion coating. (Proceq SA 2016) A problem might be to get low resistivity in the concrete, for the measurements, if moisture is stopped by the impregnation.

4. Methods of characterization

4.1. Table of investigations

On Moholt Bridge a detailed investigation was performed. Cecilie Bridge was investigated after that. The investigation in Cecilie Bridge was a smaller investigation. The priority was on obtaining some results, without doing the most time-consuming work. The result would also make a basis for deciding on further investigations or not. An overview of the work done on each bridge is provided in Table 4.1.

Table 4.1 Overview of performed investigations

Bridge	Cecilie Bridge	Moholt Bridge
Investigations performed	• Drilled core • Examined chloride ingress • Examined carbonation	• Established axis system • Photo the whole edge beam • Verified crack documentation • Half-cell potential mapping • Measured concrete resistivity • Measured reinforcement cover depth • Drilled cores • Examined chloride ingress • Examined carbonation • Inspected reinforcement corrosion in drilled cores • Investigated self healing

4.2. Moholt Bridge

The first step was to do half-cell potential, resistivity and cover measurements on the bridge. Then a decision could be made on what points of interest to examine closely and take samples from. The edge beam along the bridge span was measured only. The joint on the east side and on the inside of the fence, was chosen as point (0.0 m) (Figure 4.1). A 50 meters long measuring tape following the curve of the beam was used as the axis. Close pictures were taken along the whole span. Before taking pictures, the stirrups where located and marked. An example is given in Figure 4.2. After measurements were done, the next step was to drill cores for testing in the laboratory with μ-XRF.

Figure 4.1 Point 0.0 m for the established axis along the norther edge beam of Moholt Bridge is to the right in this picture. It's a little bit hard to see in the picture, but the measuring tape follows the the 45-degree edge bevelled by a 20 mm lipping.

Figure 4.2 Another picture of the axis, the stirrups are marked. In this picture point 6.61 m is located, that is where later core B was drilled from. At 6.61 m the tiny 0.15 mm singular crack is hard to see, even on a close up picture. The cracks with a darker color is the map pattern type of cracks.

4.2.1. Half-cell potential measurements

Half-cell potential measurements were done in compliance with the guidance from NPRA field manual (NPRA 15.551 1997). Measurements were performed against a $Cu/CuSO_4$ reference electrode. A connection to the reinforcement was established at the west end of the bridge span. By first drilling through the concrete until hitting the reinforcement, then a smaller hole was drilled in the reinforcement to connect the electric cable. Another hole was drilled to a stirrup on the east end, around 44 meters away. The resistivity was checked with a multimeter and the connection was god. The resistance should be lower than 1.0 Ωm according to NPRA guidance for half-cell potential. The fence was also confirmed to be connected to the reinforcement.

The first day doing half-cell potential measurements at the bridge, 15 February 2017, the potential was measured at every stirrup for the first 5 meters with the $Cu/CuSO_4$ rod. A device called *Proceq Profometer Corrosion* was used. The temperature was from 0 to 3 degrees Celsius, the air was dry and the sun shined, but later some clouds added to. The previous days had been almost the same, with a varying temperature between -4°C to +5°C and dry weather. A log of the weather conditions is provided in Appendix B. The concrete surface was moistened before measuring. Since prewetting is needed if the measured value of the corrosion potential changes or fluctuates with time (ASTM 876-15 2015).

Figure 4.3 Measuring half-cell potential with the Profometer, here the Cu/CuSO4 rod is used in combination with the Proceq Profometer.

More half-cell potential measurements were done two days later, 17 February 2017. This time the temperature was a little bit higher, 2°C – 5°C. It was raining and the concrete was wet. Using the wheel, a half-cell potential map of the whole edge beam was generated with

a distance of 5 cm between each measured point. To check the reproducibility some areas were additionally measured with the rod. The figure where measurements with the rod and the wheel are plotted together, is provided in Appendix C, Figure 10.7. Both the rod and the wheel uses $Cu/CuSO_4$ half-cell solution. Connection was checked with a multimeter. The area on the edge beam, inside the fence, is so narrow that there was only room to measure along one line with the wheel, so the measured area is around 46.85 meters long and only 0.05 m wide. The cross section of the edge beam is provided in Figure 4.4.

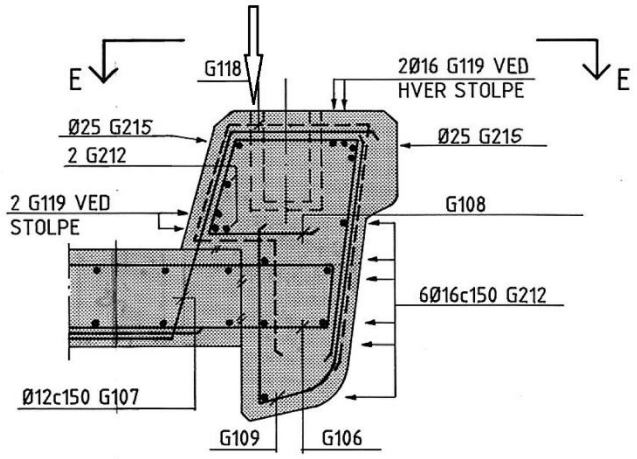

Figure 4.4 Cross section of the northern edge beam. The arrow indicates where on the cross section the half-cell potential measurements were done and the cores drilled.

Measured half-cell potentials were saved on the measuring device. It was later extracted using the provided software from *Proceq*. Example of the data in the software are provided in Appendix C Figure 10.8 and 10.9.

4.2.2. Concrete cover measurements

Cover measurements where performed using a device from *Proceq* called *Profometer.* First the stirrups where located and marked along the edge beam. At the same time, there was an attention to cover depth. To get correct cover depth, the *Profometer* need reinforcement diameter as an input. The drawings said the stirrups had a diameter of 12 mm. And the expected cover depth, from the drawings, is 50 mm. For areas where the cover depth deviated from the drawings a reference cover depth was noted. There was not discovered sudden changes in cover depth. It should be noted that there is quite a distance between some of the noted measurements. That's due to a problem with saving in the *Profometer* because the device sometimes restarted for no reason. And it was hard to make many written notes because of the rain.

4.2.3. Resistivity measurements

Resistivity in the concrete was measured with approximately one meter distance between each measurement. A device from *Proceq* called a *Resipod* was used. It needs at least 150 mm spacing between the reinforcement for a proper measurement. Or else we need to consider that the low resistivity of the reinforcement changes the results. Therefor the measurements were done diagonal in the square between the stirrups and the longitudinal reinforcement (Figure 4.5). The device was calibrated using a plate with known resistance

before measuring. Two points where measured each time. One in the square between the longitudinal reinforcement bellow the fence and the longitudinal reinforcement along the pedestrian path, and one point between the longitudinal reinforcement bellow the fence and the longitudinal reinforcement at the outer edge of the bridge. When choosing were to measure, the focus was on choosing places where the distance between the reinforcements gave most room. A note was added to values that were uncertain because of narrow space. In general, it was more room to measure between the reinforcements on the outer side of the fence. The whole bridge was measured 17 February 2017. But some measurements were also done 15 February 2017, when the weather was dryer and colder, for comparison.

Figure 4.5 Measuring resistivity diagonal within reinforcement marked with crit. The picture show a measurement on the outer side of the fence, the inside area between the fence and the pedestrian lane mas measured in the same way. The device is a Proceq Resipod.

4.2.4. Visual inspection

A visual inspection was performed. Photos were taken along the whole northern edge beam of the bridge. Location of the stirrups and the axis system is included in the photos.

Crack width are based on the report from August 2015. (Skare and Stemland 2015) From the photos along the bridge, it was confirmed witch of those cracks were still visible in February 2017. But it was not possible to measure the crack width from the photos. Therefore, the crack width from the report was assumed. Cracks where the cores were drilled was checked again with a crack width ruler.

4.2.5. Drilling cores

Drilling cores was done by Ove Loraas at NTNU concrete laboratory. It was done according to the guidance given by NPRA. (NPRA 15.516 1997) By advice of Ove the core diameter was chosen as 80 mm, instead of 100 mm as suggested by NPRA. The decision to drill 5 cores was made based on the measured data, and the plan is given in Table 5.2. The available equipment was not suited for drilling on the narrow edge beam, therefore only three of the planned cores were drilled.

4.2.6. Characterization of carbonation depth

Thymolphthalein is sprayed on the fresh cores right after drilling on the bridge. This is done to check carbonation depth. The core is very wet from the cooling water during the drilling. Before spraying the core, it was dried with a cloth so that it was just dry enough to prevent the thymolphthalein to flow. Thymolphthalein shift the color where there is no carbonation to blue. Then the distance from the surface down to the blue color is measured with a ruler.

4.2.7. Characterization of chloride ingress

The µ-XRF instrument at Department of Structural Engineering, NTNU was obtained in November 2016 through funding from NTNU, and the instrument is still being tested (June 2017). The µ-XRF instrument detects counts per second/eV (number of fluoresced X-rays in a certain energy window). To determine concentration, a calibration curve is to be established using a set of reference standards. With µ-XRF it is not possible to detect elements with an atomic number lower than 11 (Na). That means that elements like e.g. O and H are not detected. Measurements appear normalized to the mass of the following elements: Ca, Si, Al, Fe, Na, K, Mg, Cl, S, P, Ti, Mn, in the volume measured. The suggested unit to use is [elemental mass %xrf]. (Danner 2017)

µ-XRF was used to study the chloride ingress in the concrete cores. Before that the core was cut in half, using a water cooled saw blade. That was done to have a fresh concrete surface. Only one half from each core was tested in the µ-XRF. The other half is saved for later and could possibly be used for other test methods.

The half was investigated with a M4 Tornado µ-XRF apparatus from Bruker. The instrument uses a silicon drift detector energy dispersive spectrometer (SDD-EDS). The µ-XRF is equipped with a silver X-ray tube and polycapillary lenses focusing the X-ray beam to a spot size of 25µm. For point analysis, a current of 200 µA and a voltage of 50 kV were used. For line scans and elemental mapping the current was increased to 600 µA. The chamber pressure was 20 mbar at all times. (Danner et al. 2017)

4.2.8. Investigate self healing

When testing the cores in the µ-XRF, detecting high concentrations of calcium and magnesium in cracks, indicate self healing, were also done. (Savija and Schlangen 2016)

4.3. Cecilie Bridge

4.3.1. Drilling core

After a visual inspection, a core from the edge beam next to the pedestrian lane, was drilled. The core was drilled almost in the middle of the bridge, approximately 62 m from the east end of the bridge. This is one of the places where the distance from the edge beam to the driving lane is shortest. There is a 0.45 mm wide crack where the core is taken, but no reinforcement. The focus was to check chloride ingress, not reinforcement corrosion. It was therefore decided to drill beside the reinforcement since. It is easier to drill a core when not drilling through the reinforcement. The drilling was performed by Ove Loraas from NTNU concrete laboratory. The guideline from NPRA was followed, except that the core diameter is 80 mm instead of 100 mm (NPRA 15.516 1997).

4.3.2. Locating reinforcement

When locating the reinforcement to establish an electrical connection for the half-cell potential measurements, cover depth was measured to find the place with lowest cover depth. In general, the cover depth was around 70 mm both for the stirrups and the longitudinal reinforcement. The lowest located cover depth was around 40 mm. This place was chosen for an attempt to drill down to the reinforcement for the electrical connection, but it was not discovered any reinforcement there.

4.3.3. Resistivity measurements

In the area where the core was drilled, resistivity was measured before and after. But the results are not considered reliable because the moistening was too varying because of the cooling water from the machine that drilled the cores.

4.3.4. Visual inspection

The bridge was inspected and photos were taken. Some of the singular cracks were measured before deciding where to drill core A.

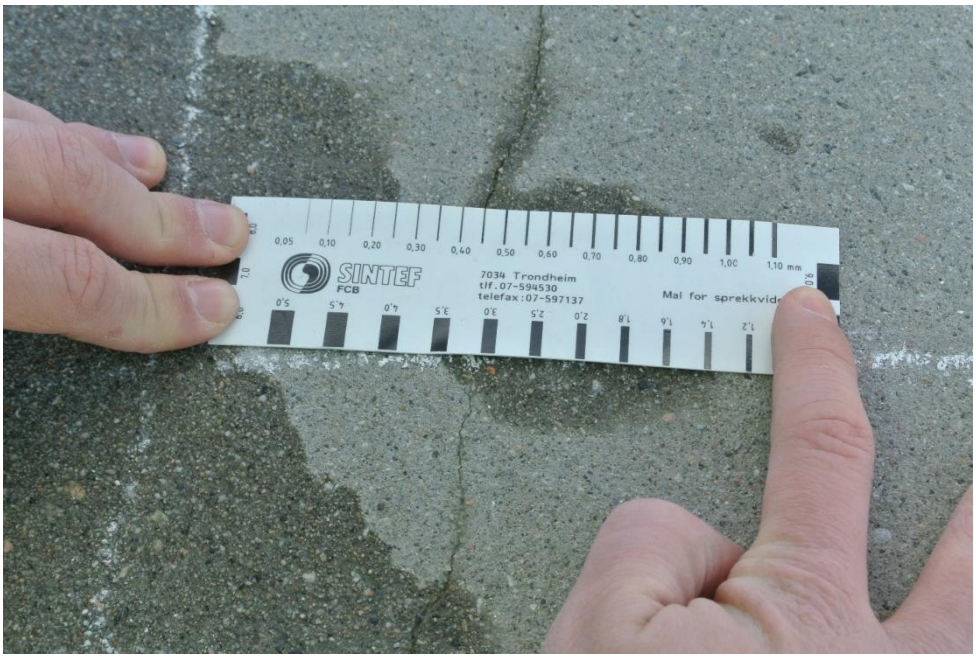

Figure 4.6 Measuring crack width where core A from Cecilie Bridge later was drilled.

4.3.5. Characterization of carbonation depth

Core A was sprayed with thymolphthalein right after drilling on the bridge to check carbonation. Before spraying the core was dried enough that the thymolphthalein did not flow. Since it was such a small carbonation depth the crack width ruler was used to measure it.

4.3.6. Characterization of chloride ingress

µ-XRF was used to study the chloride ingress in the concrete core, that was performed following same process as described on Moholt Bridge (Chapter 4.2.7).

5. Results

5.1. Moholt Bridge

5.1.1. Measurements prior to drilling the core

Since there are so many measurements, the half-cell potential measurements are presented in graphs instead of table for a better overview. For closer examinations, original values for half-cell potential and resistivity measurements are provided in Appendix C.

Figure 5.1 the half-cell potential and resistivity measurements from 0 – 3 m on dry and wet concrete. The plotted potential in Figure 5.1 is an average of three measurements over the same area, reducing the impact of an erroneous measurement. Both half-cell potential and concrete resistivity was lower in the wet than in the dry concrete. The average half-cell potential was -8 mV and average concrete resistivity was 79 kΩcm in the dry concrete. In the wet concrete average potential was -95 mV and average resistivity was 15 kΩcm.

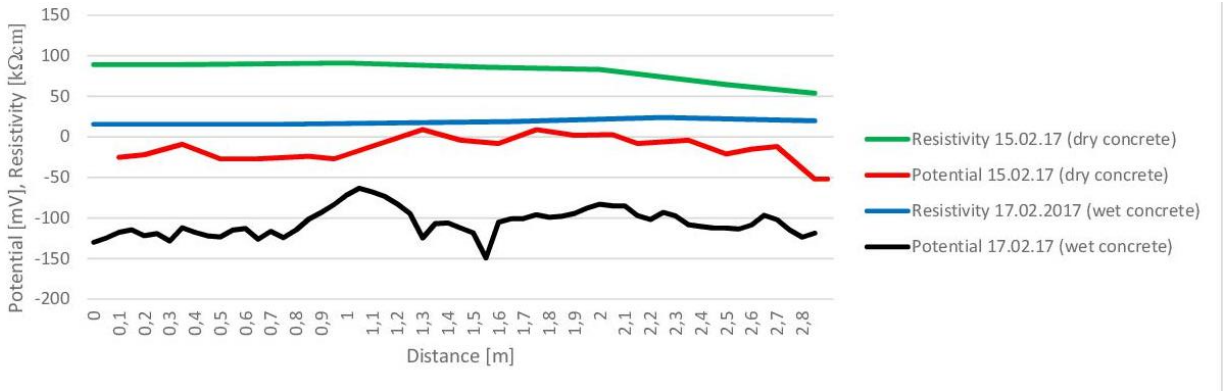

Figure 5.1 half-cell and resistivity measurements done on wet (17.02.17) and dry (15.02.17) concrete for the first 3 meters of Moholt Bridge. X-axis represent distance from point 0, given in meters. Point 0 is at the east end of the bridge, as shown in Figure 4.1

Figure 5.2 shows an overview of half-cell potential, concrete resistivity and reinforcement cover depth measurements along the whole span of the edge beam from Moholt Bridge. Crack distribution and crack width is also included. The plotted potential in Figure 5.2, is smoothed out by using the moving average of three values. Hereby an erroneous measurement point might be removed. On the other hand, by removing sharp peaks, some detailed information could be lost. When examining the results closely, both a comparison and a closer look at the original values are important. Original values are provided in Appendix C.

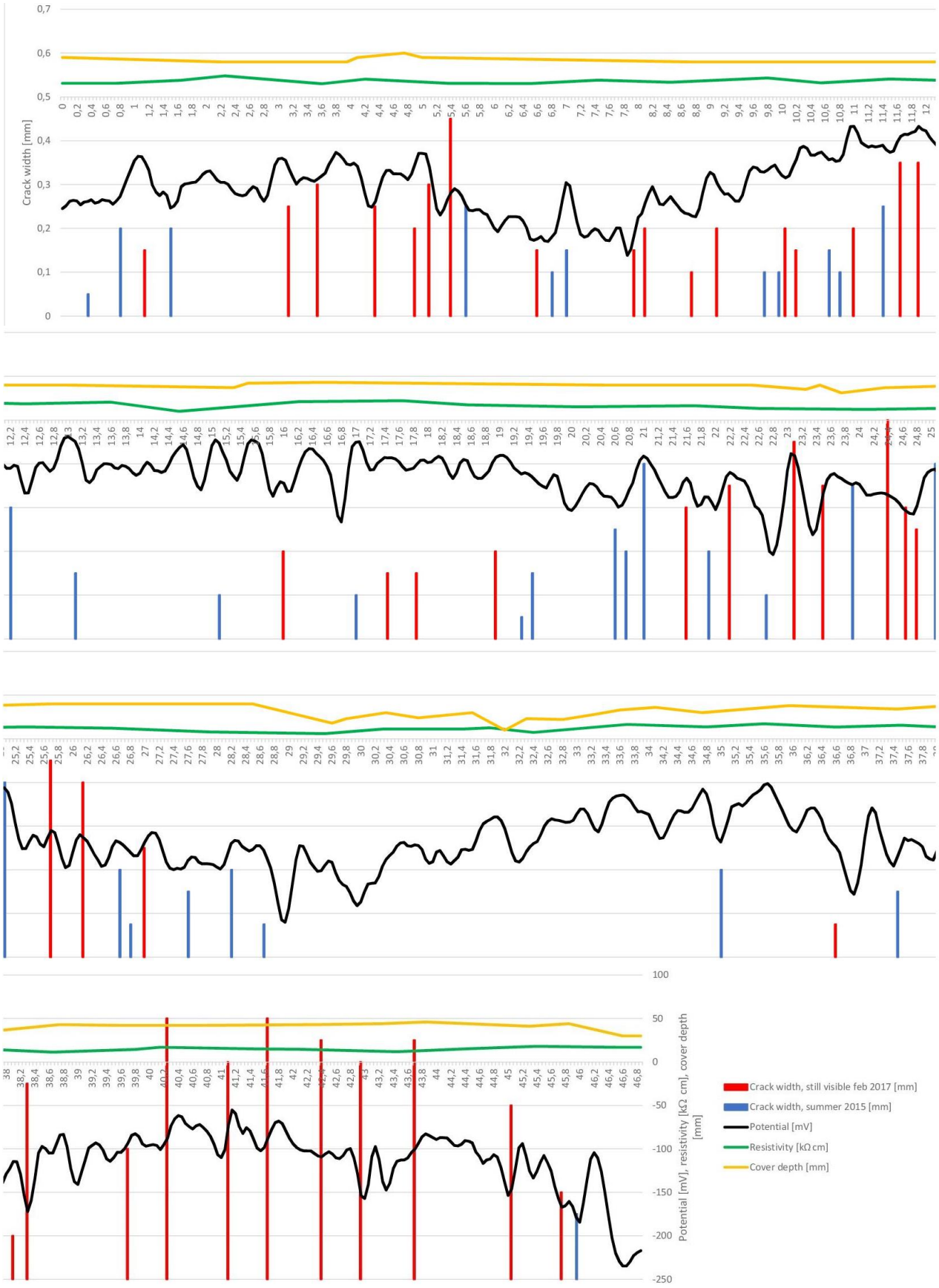

Figure 5.2 Complete measurements from Moholt Bridge, half-cell potential, concrete resistivity, cover depth and crack width together. The x-axis starts with 0 m at the joint on the east side and ends at 46.85 m at the joint on the west side of the bridge. The reference electrode is a Cu/CuSO₄.

From the Figure 5.2 it can be seen that the potential varies from -19 mV to -235 mV with an average of -98 mV. One trend is a distinct peak up and a peak down reading almost every two meter from 1 m to 45 m and at 46 m. These peaks fall together with the location of the steel post for the fence. This is easier to see in the diagram with the original values, provided in Appendix C, fig 10.3. No pattern between crack distribution and potential values were discovered. The location of cracks coincided both with regions of high and low half cell potential.

The concrete resistivity in Figure 5.2 varied between 6 kΩcm and 24 kΩcm, but most of the values are close to the average of 15 kΩcm. The day the measurements were taken the temperature was 5°C. Reducing the temperature by 1°C increases the resistivity of concrete by up to 5% (Polder et al. 2000). Consequently, the average resistivity would be about 8.5 kΩcm at 20 °C. There is an area from 27m to 30m with low half cell potential values (-150 - -200mV). In this area, a large sign is fixed to the edge beam by three connections.

The specified cover depth is 50 mm. The measured cover depth shows many lower values. Mostly around 40 mm, but a larger area around the sign fixing, 27.0 m – 30.2 m, have many values around 20 mm. The lowest value is 10 mm. The cover depth of the reinforcement measured on the bridge, as plotted in Figure 5.2, compared to the exact cover depth measured from the drilled cores are provided in Table 5.1.

Table 5.1 Measured cover depth, using cover meter, compared to real cover depth

	Measured on the bridge	Measurement certainty	Real depth measured on drilled core
Core A	40 mm	High, measured and noted exactly, but not repeated	40 mm
Core B	45 mm	Low, measured, but repeated and noted 2,1 m and 1,6 m away	66 mm
Core E	43 mm	High, measured, repeated and noted exactly	49 mm

In Table 5.2 the overview of the planned concrete cores from Moholt Bridge is provided. Core C and core D were not drilled.

Table 5.2 Plan for drilling cores on Moholt Bridge

Core number	Location	Crack width	Half cell potential	Cover depth	Concrete resistivity	Note
A	2,16 m	No crack	- 100 mV	40 mm	20 kΩcm	Reference core, no crack
B	6,60 m	0,15 mm	- 150 mV	45 mm	15 kΩcm	Narrow crack, low HCP
C	10,20 m	0,15 mm	- 75 mV	40 mm	15 kΩcm	Narrow crack, medium HCP
D	Choose one on site					Map pattern crack
E	42,40 m	0,55 mm	- 100 mV	43 mm	15 kΩcm	Wide crack, medium HCP

5.1.2. Self healing

No indication on self healing was seen in the cores, neither due to visual inspection nor due to the mapping of the elements in the cracks using the µ-XRF.

5.1.3. Carbonation

Core A and core B from Moholt Bridge was checked on site, right after the cores were drilled. Core A didn't give reliable results because too much thymolphthalein was used. Core B gave clear results. The carbonation depth was measured to be in average 3 mm in core B (Figure 5.3).

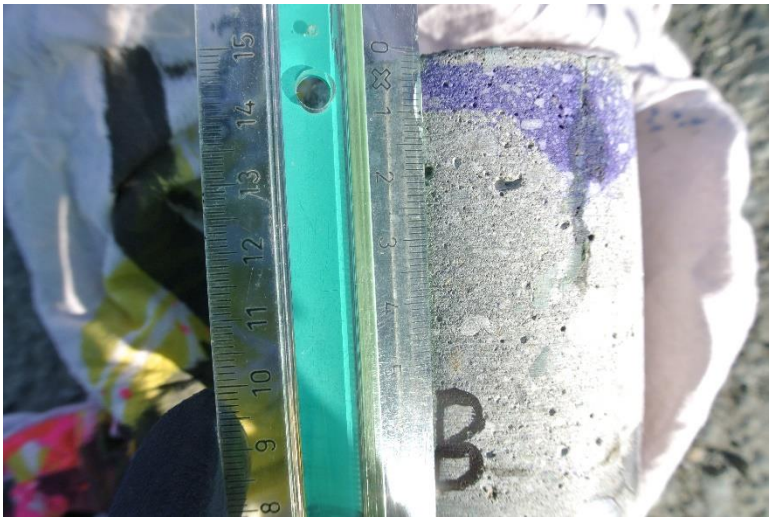

Figure 5.3 On site checking of carbonation depth at Moholt Bridge, core B

5.1.4. Chloride ingress

The cores were characterized with the µXRF. The main thing to remember regarding the µ-XRF and chloride mapping, is that the distinct color intensities are only comparable within the same picture. Effort have therefore been made to locate the highest Cl concentration in each sample to know what the intensities are compared against. A false color scan shows normalized intensities and is provided by the µ-XRF software (Figure 5.10).

5.1.4.1. Core A

Figure 5.4 Mosaic picture of core A, Moholt Bridge. Exposed concrete surface is on the top.

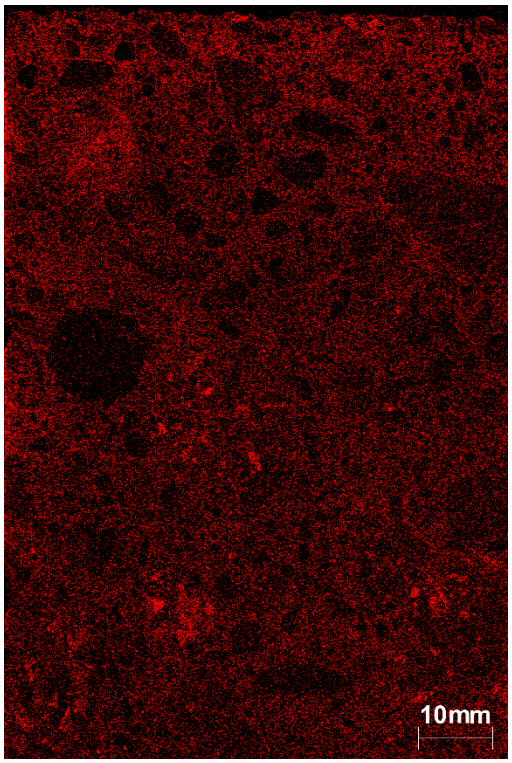

Figure 5.5 Chloride mapping of core A, Moholt Bridge. Exposed concrete surface is on the top.

Figure 5.4 and Figure 5.5 show a mosaic picture of concrete core A and a chloride mapping of the area marked in Figure 5.4, respectively.

The chloride mapping of Core A shows no areas with more distinct concentration, except a little more distinction closest to the top surface.

5.1.4.2. Core B

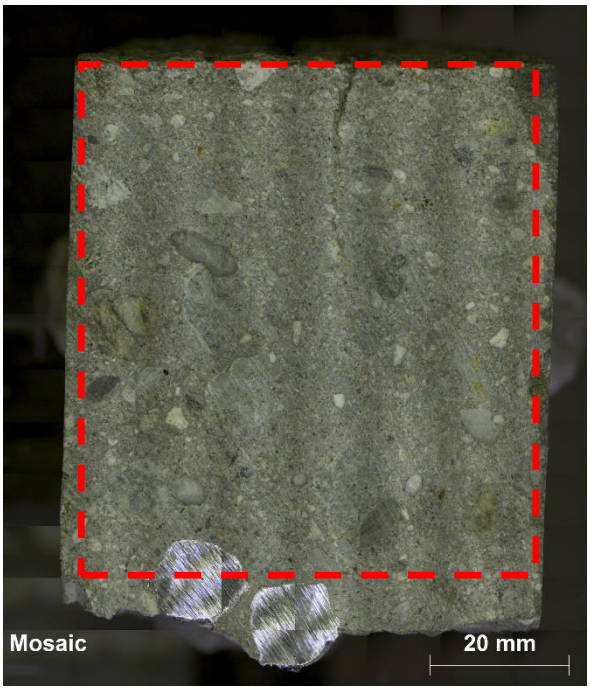

Figure 5.6 Mosaic picture of core B, Moholt Bridge. Exposed concrete surface is on the top.

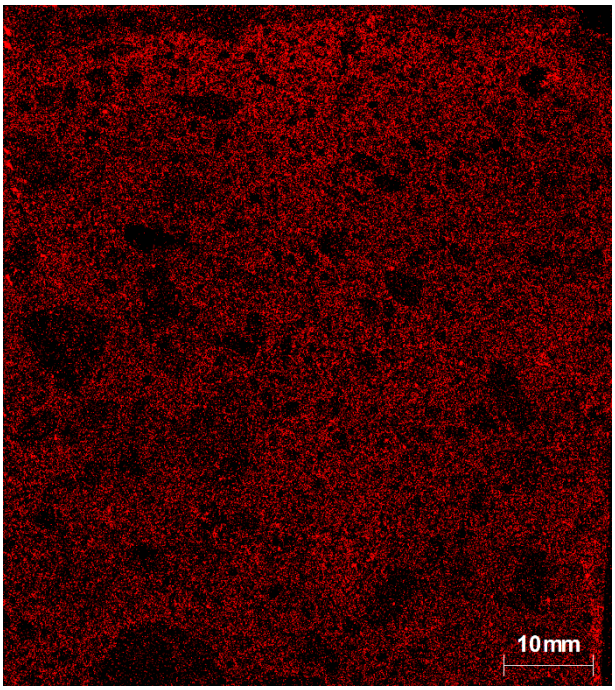

Figure 5.7 Chloride mapping of core B, Moholt Bridge. Exposed concrete surface is on the top.

Figure 5.6 and Figure 5.7 show a mosaic picture of concrete core B and a chloride mapping of the area marked in Figure 5.7, respectively.

The chloride mapping shows no areas with more distinct concentration, except a little more distinction closest to the top surface. The small crack in this core, does not extend deep, it was closed before it reaches the reinforcement.

5.1.4.3. Core E

Figure 5.8 Mosaic picture of core E, Moholt Bridge. Exposed concrete surface is on the top.

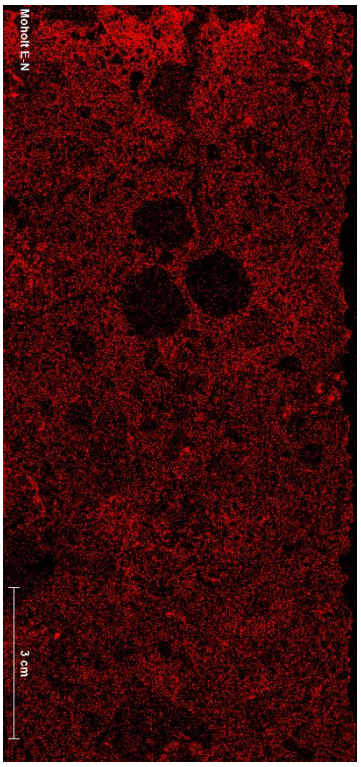

Figure 5.9 Chloride mapping of core E, Moholt Bridge.

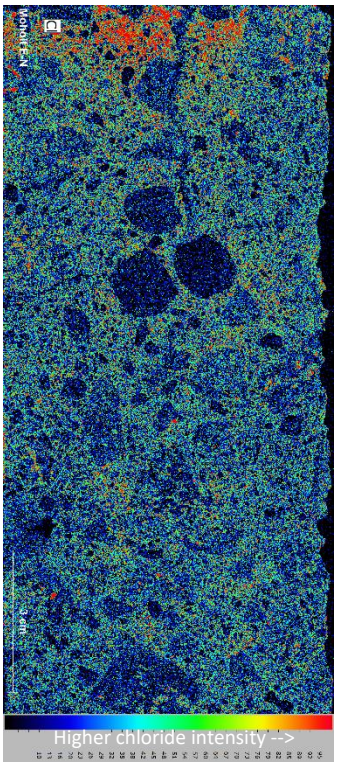

Figure 5.10 False color chloride mapping of core E, Moholt Bridge. Red color indicating highest chloride intensities.

Figure 5.8 and Figure 5.9 show a mosaic picture of concrete core E and a chloride mapping of the area marked in Figure 5.8, respectively. Figure 5.10 shows a false color chloride mapping of core E. In the false color chloride mapping intensities are defined by colors. Red colors indicating high intensities and blue colors indicating low intensities.

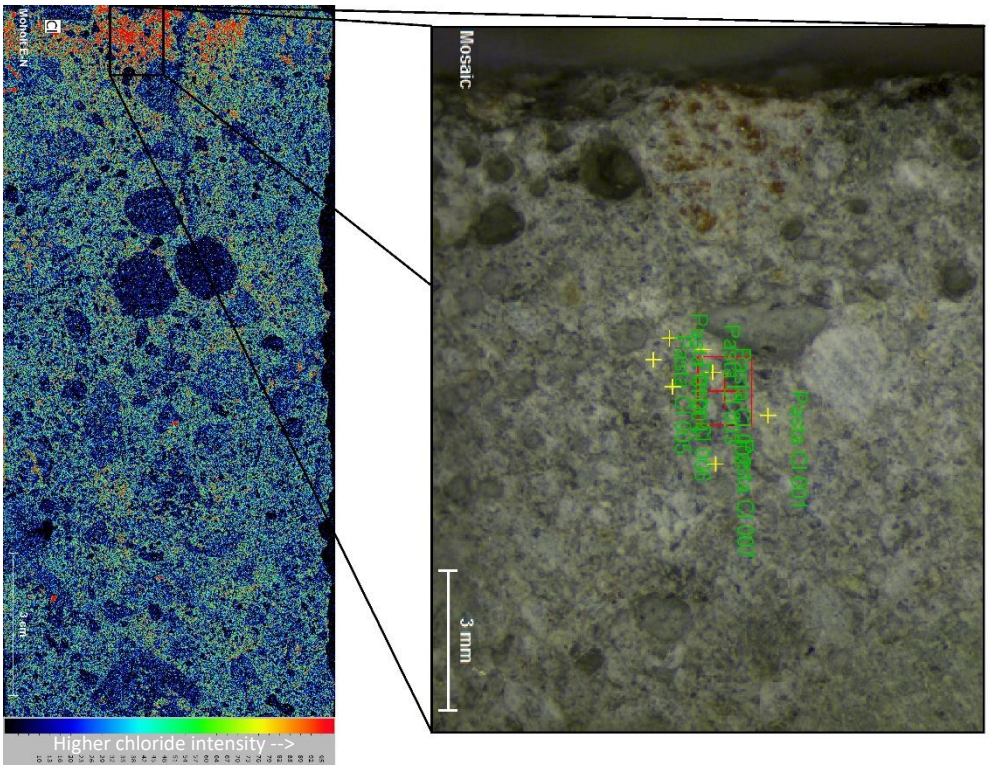

Figure 5.11 Placing of the measured points in core E.

Bruker Nano GmbH, Germany

M4 Tornado

Quantification results

~~Mass percent (%)~~ elemental mass %xrf

Date: 04/04/2017

Spectrum	Na	Mg	Al	Si	S	Cl	K	Ca	Ti	Mn	Fe	Ag
Pasta Cl 0	0	2,076415	3,372217	17,95234	1,288495	0,360767	0,14278	63,7013	0,801666	0,168612	10,13541	0
Pasta Cl 0	0	1,252672	2,13799	13,70877	0,963436	0,196962	0,105196	73,02372	0,483577	0,168054	7,959623	0
Pasta Cl 0	0	0,871094	2,226117	30,50749	1,998815	0,089731	0,5422	56,75845	0,34245	0,119489	6,544163	0
Pasta Cl 0	1,214795	1,261441	6,128729	22,83551	1,943131	0,12346	0,415691	59,7677	0,375834	0,123001	5,810709	0
Pasta Cl 0	0,121495	1,097777	2,92164	13,47546	2,5542	0,216866	0,121228	71,94396	0,288272	0,096907	7,162192	0
Pasta Cl 0	1,427088	2,96619	7,227108	23,70971	1,673108	0,151119	0,180198	46,23553	0,873402	0,272009	15,28454	0

Table 5.3 Measured elemental concentration in elemental mass $\%_{xrf}$ in specific points on Core E shown in Figure 5.11.

In the area of highest chloride intensities from the false color scan, single point analysis was performed to investigate the highest chloride content. The location of the point analysis is shown in Figure 5.11.

The results of the elemental analysis of each measured point in [elemental mass $\%_{xrf}$] is given in Table 5.3.

Highest found chloride concentration was 0.36 elemental mass $\%_{xrf}$, located 8 mm from the exposed surface. In the false color scan, it could look like there is a deeper ingress around the crack. However, note that on the right side of the crack, a large aggregate is responsible for an area without any chlorides. This could contribute to create the visual impression of more chloride around the crack. It could still be argued that the ingress is deeper where the crack is, but that would be a weak statement.

5.2. Cecilie Bridge

5.2.1. Cracking

Measured cracks on Cecile Bridge seem to be continuous through the sides and the top surface. The crack width varied between 0.30 mm and 0.45 mm, but this only represent a few cracks that were measured before deciding where to drill core A.

5.2.2. Chloride ingress

Results from the characterization of core A from Cecilie Bridge, with the µ-XRF, are shown in Figure 5.12-5.15.

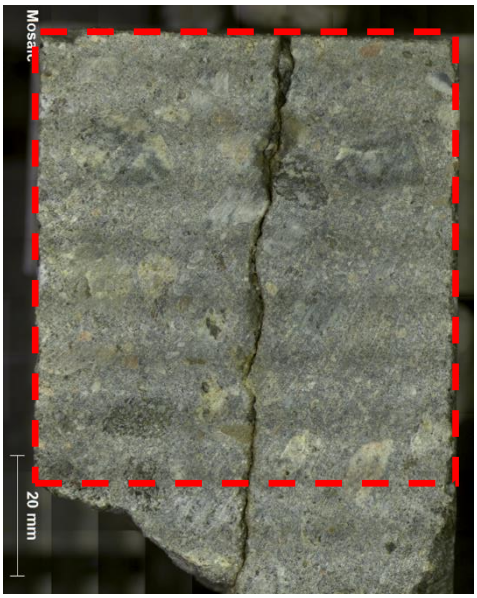

Figure 5.12 Mosaic of Core A, Cecilie Bridge. Exposed concrete surface is on the top.

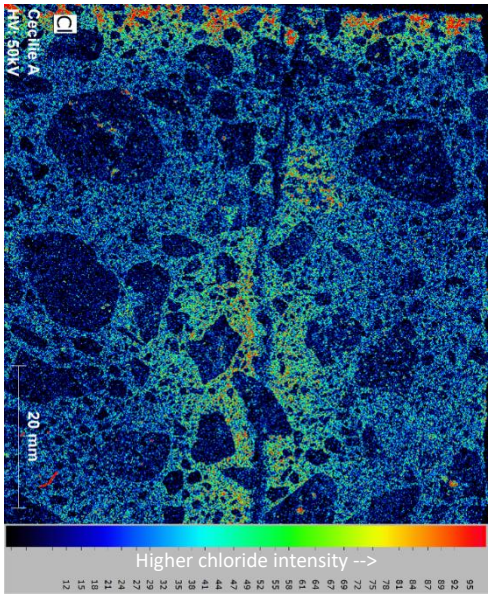

Figure 5.13 False color chloride mapping for core A, Cecilie Bridge. Exposed concrete surface is on the top.

Figure 5.12 and Figure 5.13 show a mosaic picture of concrete core A and a false color chloride mapping of the area marked in Figure 5.12, respectively. In the false color chloride mapping intensities are defined by colors. Red colors indicating high intensities and blue colors indicating low intensities.

The false color chloride mapping shows that there was a chloride ingress both from the top surface and from the crack surface. Except a little area from 0.7 cm to 2.0 cm from top, where there was no chloride ingress from the crack surface.

In the area of highest chloride intensities from the false color scan, single point analysis was performed to investigate the highest chloride content. The location of the point analysis is shown as *Object_1-5* in Figure 5.14.

The results of the elemental analysis of each measured point (Object) in [elemental mass $\%_{xrf}$] is given in Table 5.4. And the measured spectra of elements are in Figure 5.15

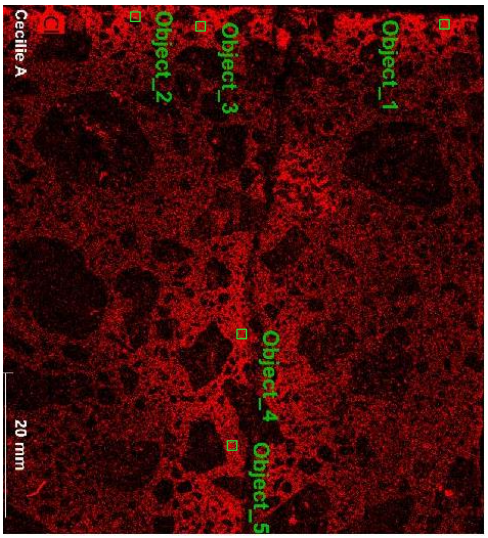

Figure 5.14 Chloride mapping and location of the measured points (Objects) in core A, Cecilie Bridge.

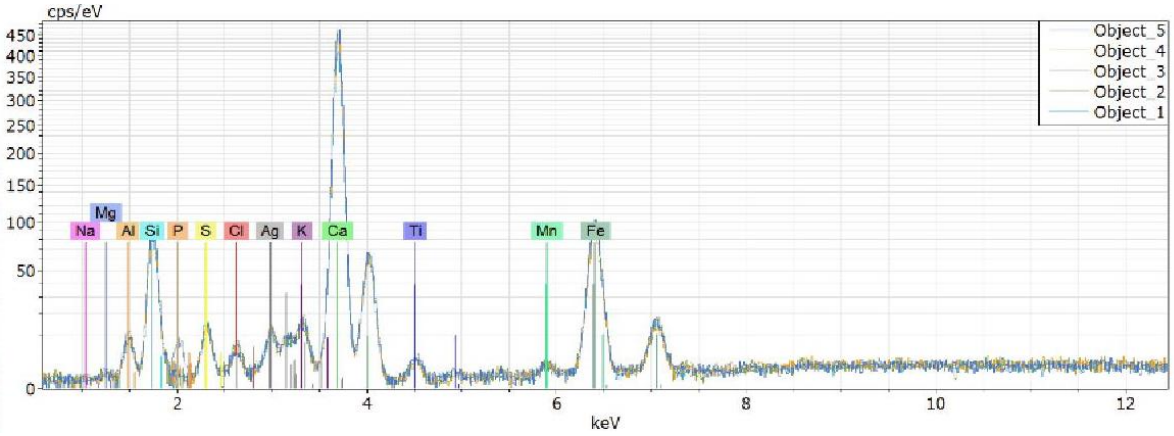

Figure 5.15 Measured spectra of elements in selected points (Objects in Figure 5.14)

Table 5.4 Elemental mass $\%_{xrf}$ of elements in selected points (Objects in Figure 5.14) in core A, Cecilie Bridge.

~~Mass percent (%)~~ elemental mass %xrf

Spectrum	Na	Mg	Al	Si	P	S	Cl	K	Ca	Ti	Mn	Fe
Object_5	0.00	0.15	4.66	24.60	0.00	1.50	0.14	1.07	59.85	0.51	0.10	7.41
Object_4	0.00	0.00	4.78	23.61	0.00	1.42	0.16	1.24	61.49	0.40	0.11	6.79
Object_3	0.00	0.84	5.37	23.06	1.27	1.28	0.19	1.55	58.21	0.65	0.11	7.48
Object_2	0.00	0.76	4.44	25.08	0.00	1.43	0.29	1.03	59.10	0.34	0.10	7.43
Object_1	0.00	0.12	5.14	23.56	0.00	1.64	0.33	1.44	59.31	0.56	0.14	7 .77

Highest found chloride concentration in the core was 0.33 elemental mass $\%_{xrf}$ at Object_1. The penetration depth was almost the same around the crack as from the top surface. Except, there was an area around the crack from 0.7 cm to 2.0 cm, right underneath the ingress from the top surface, that does not contain any chloride.

5.2.3. Carbonation

Core A was sprayed with thymolphthalein, this showed a carbonation depth of 1 mm (Figure 5.16).

Figure 5.16 Checking carbonation depth on core A at Cecilie Bridge.

6. Discussion

The discussion consists of two parts. Chapter 6.1 and 6.2 discuss the methods and results from half-cell potential, cover depth and concrete resistivity measurements. Chapter 6.3 and 6.4 assess the chloride ingress and reinforcement corrosion, which are the main objectives in this project.

6.1. Investigation at Moholt Bridges

6.1.1. Cracks

The motivation for knowing witch crack mechanisms occurring, is the relation to exposure from development time and crack characterization. Described in chapter 3.2.5, two types of cracks were observed at Moholt Bridge. One type of crack forming a map pattern and one type of crack that was longer and singular. Visual inspection, documentations and reports from the bridge is used to identify the reason for the cracking. Information on different crack types is given in Appendix D.

First the cracks in a map pattern (Figure 4.2). The report by Skare and Stemland (2015) identified these cracks to be due to plastic shrinkage. According to the bridge data from NPRA, the cracks are due to ASR. Knowing when the cracks developed would settle that, but that information was not found. After examining core E, it was noted that the way the core dried up after drilling , could indicate micro cracks due to ASR damage (Figure 6.1). Further investigations with the µ-XRF could not find any evidence for ASR. Higher concentration of K, Na and silica around aggregate or in cracks within the aggregate were not found (Danner 2017). Even though no visible evidence (e.g. gel formation) was found, it does not rule out ASR damage (Geiker 2017). A conclusion was not reached on this topic.

Figure 6.1 A picture of core E, Moholt Bridge. It is oriented so that the surface is on top in this picture. This picturce is taken right after the core was drilled and therefor it had recently been exposed to a lot of water needed to cool the drilling equipment.

The second type of cracks, the singular ones (Figure 6.2)**,** were continuous both on the sides and the top surface of the edge beam. They probably developed due to a combination of several mechanisms. Possible mechanisms are external restraint due to temperature differences, since the edge beam and the slab were not cast at the same time. Other likely mechanisms could be loading, drying shrinkage and autogenous shrinkage. This means the cracks should have developed within the first months. The fact that they go around and not through the aggregates in our examined cores, amplifies this assumption of an early crack development. The cracks probably developed before the paste had high enough strength to guarantee bounding to the aggregates.

Figure 6.2 One of the singular cracks. This picture is from the outer side of the edge beam. This crack extends on the top surface to where core E was drilled.

The crack distribution was more intense above the supports of the bridge. That makes sense since there also is a strain on the top of the beam in that area due to the loading. The difference in the observed crack distribution between summer 2015 and February 2017 could be because some cracks have closed and due to different approaches on which cracks to include in the mapping. Only long singular cracks, visible both on the side and the surface, where included in February 2017. It is interesting that some of those cracks are located between the stirrups, some are right on top of a stirrup and some are almost parallel to and

then cross the stirrups. A crack that crosses the stirrup perpendicularly would probably lead to macro-cell corrosion, a crack moving parallel to the stirrup could also lead to uniform corrosion (Elsener et al. 2003).

The crack history might have an impact on chloride ingress. There can be much information extracted in comparing the chloride ingress in a ASR crack with a singular crack, since it is expected that there are typically 15-20 years difference between the time they developed (Rodum 2010). This could give valuable information on the development of chloride ingress in cracks during the service life of the bridge. This is something to be conscious of in later studies. In this study only cores with the second kind of cracks, the singular ones, where obtained and examined. That was because the equipment available was not suited for drilling on the narrow edge beam at Moholt Bridge. Therefore, only three of the five planned cores were drilled. The priority was to obtain cores representing different cracks width and a reference core with no crack. Although, the drilled core E indicated that there might be other crack types than the singular one, that was the focus of investigation in that core.

6.1.2. Exposure

The downslope of the bridge, might lead de-icing salt to flow away from the northern side of the bridge, potentially reducing the transport of chlorides into the concrete. Opposite to that, the main wind direction and splashing from tires is expected to contribute to the salt transport from the driving lanes to the edge beam (Figure 3.3 and 3.4). There is still some uncertainties regarding the exact exposure of the bridge. The driving lanes on the bridge probably have high exposure, but the investigated northern edge beam is expected to be the least exposed. This conclusion is based on the distance to the regularly salted driving lanes (4.0 m), with regard to the mentioned factors on chloride transportation.

Obtaining necessary data on chloride exposure was not successful. Because of that, it was not done any calculations on what chloride ingress to expect by using the error function of Fick's second law. In the future, it might be beneficial to use a different approach than search for historical data on use of de-icing salt, when determining the chloride exposure.

6.1.3. Half-cell potentials

The distinct half-cell potential peaks every two meter fall together with the steel posts of the fence, which is embedded in the concrete. An outtake of the HCP diagram, without moving average, is provided in Figure 6.3**.** There is a fence post at 23 m and 25 m in that figure. The whole diagram is provided in Appendix C. It is established that the steel posts are in connection with the reinforcement. The steel posts might interfere with the measurements. On the other hand, it could also be possible that there is some corrosion in these points. "Potential differences of around +100 mV within 1 m measure area, together with negative potentials can be a clear indication of active corrosion" (Proceq SA 2016). The peak down with low values indicate the location of an anode and then the steel around acts as a cathode, as illustrated in Figure 2.3 (Elsener et al. 2003). It is visible around the posts that extra concrete has been added after the original casting (Figure 3.5). The connection between two different layers of concrete could act as a crack. No cores were drilled close enough to the fence post that this could be examined further.

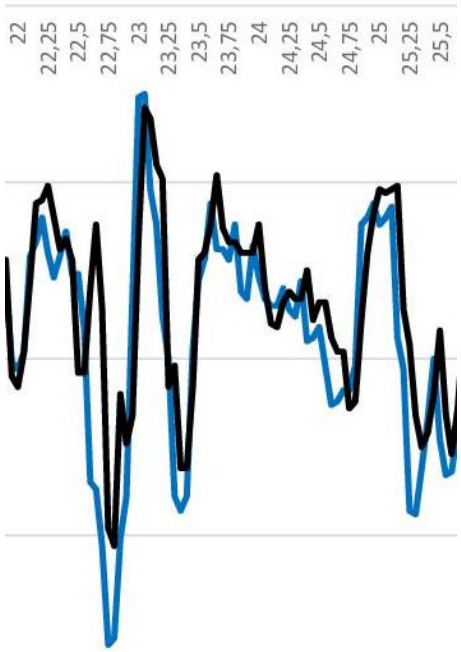

Figure 6.3 Half-cell potential values at Moholt Bridge from 22.0 m - 25.5 m.

Resistivity and half-cell potential from Moholt Bridge are plotted together in Figure 6.4, since resistivity influence the half-cell potential measurements. This gives an overview when there are many measurements. Two distinct population in Figure 6.4 could indicate that two different corrosion states are represented in the structure (Elsener et al. 2003). Figure 6.4 only show one population, indicating a coherent state in the structure. Still a span from -150 mV to -50 mV can be the difference from active to passive corrosion (Procceq 2016). There is one point with low half-cell potential value (-220 mV) that stands out from the rest. It was not possible to measure resistivity very close to the fence post, so there could be another population around the fence post which is not shown. This graph therefore only represents the area between the posts. Temperature affects the measurements through the change in resistivity, and therefore considered in the resistivity measurements.

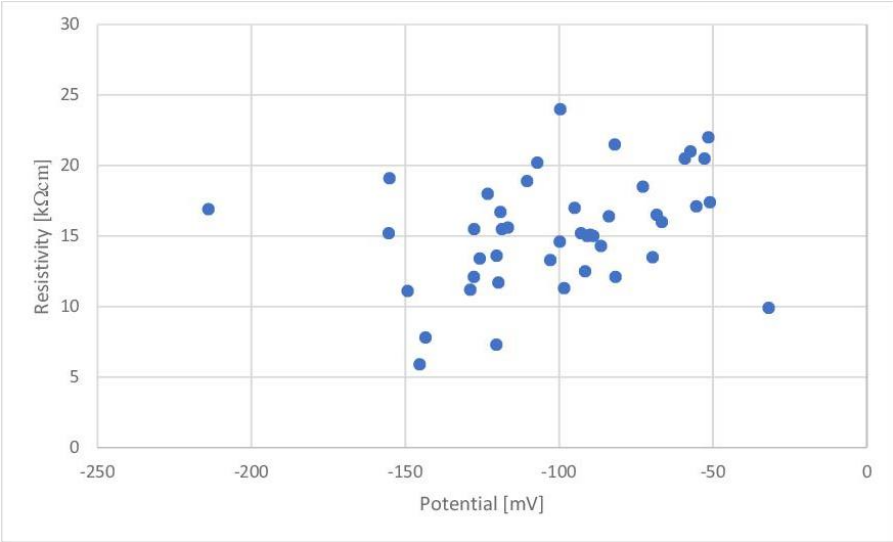

Figure 6.4 Resistivity versus half-cell potential from Moholt Bridge

6.1.4. Cover depth

When we compare the measured cover depth with the real cover depth from the drilled cores, the measurements gave similar or lower results than the real cover depth. The difference between real and measured cover could be human error because, as mentioned in methods (Chapter 4.2.2), only selected stirrups where checked again after they were located. But, it should be kept in mind that while locating, it is easy for the operator to pay attention to the cover depth, since the device displays it and beeps each time a rebar is located. There could also be an error in the measurement by the device. To get correct cover depth, the device needs the correct diameter of the reinforcement. The reinforcement diameter was known from the bridge drawings and inputted correctly, but both core B and E had two reinforcements located together instead of one. Core A had only one rebar, and this is the only core where the measured cover depth was correct. Both sources of error are likely to happen. This tells us that there could be errors in the measured cover depth with the *Profometer*.

6.1.5. Conclusions on the half-cell potential mapping on Moholt Bridge

It is interesting to look at the difference in the potential measurements from dry and wet concrete in this topic (Figure 5.1). Which in our case shifted the average potential from -8 mV to -95 mV. That is definitely a factor to consider when we are comparing our results with the standard expectations. It shows the importance of taking into account the different conditions influencing the measurements when comparing results. Anyway, our measurements indicate that the risk of corrosion is 10 % or less according the threshold suggested by Appendix X1 in ASTM C876-15 (2015).

Measured concrete resistivity on Moholt Bridge (Figure 5.2), was recalculated to standard temperature (20 °C) and compared to values in Table 2.2. This indicated that according to resistivity the risk of corrosion is moderate too high. If no active corrosion is detected, this low resistivity would not make any difference. With active corrosion, low resistivity may show where corrosion is strongest.

Although the expectation to find reinforcement corrosion were low based on the results from the half-cell potential mapping, valuable information about the relation between chloride ingress and crack width can still be obtained. The chosen cores have quite similar circumstances and parameters, where crack type and width is the varying factor, which makes it perfect for getting the answers regarding crack width this project seeks.

Getting exact values for chloride ingress and reinforcement corrosion from analyzing the cores, has a value of its own. Because it gives a reference on what the measurements on Moholt Bridge is telling, and that could be used to understand later measurements on other bridges. Then taking a decision on where to examine closer would be easier.

6.1.6. Method to investigate chloride in cores

Experience from Øyvind's project showed that the µ-XRF gave the same results as spraying with an indicator (Strømme 2017). And only using the µ-XRF would not spoil the sample. The advantages of using the µ-XRF for characterization is confirmed by experience at NTNU. (Danner et al. 2017) In Cl- mapping different intensities of chloride in the surface compared

to the bulk of the concrete core can be visualized. The intensities can be displayed as a false color scan described before.

6.2. Investigation at Cecilie bridge

6.2.1. Exposure

With regard to the experiences from Moholt Bridge a different experimental approach was chosen for Cecilie Bridge. Experience showed that sufficient exposure was important to get distinct results. Since it turned out to be difficult to obtain information on the exposure history, a core was drilled early in the investigation. The core was tested in the µ-XRF to obtain information on chloride ingress. The focus was put on chloride ingress in the first place and thus a core was drilled without reinforcement.

6.2.2. Cover depth

A problem on Cecilie Bridge was how to establish electrical connection to the reinforcement. A hole had to be drilled to get an electrical connection to the reinforcement before measuring the half-cell potential. When locating the reinforcement with the *Profometer*, the measured cover depth was higher than according to the drawings. With the *Covermeter* around 70 mm cover was measured. It was not possible to drill that deep with the normal sized drill available. Another observation was that both the stirrups and the longitudinal reinforcement had the same measured cover depth, which seems illogical since they overlap each other. It is suspected that something interfered with the measurements. Therefore, the measuring device was checked on other reinforced concrete samples in the laboratory, right after measuring at Cecilie Bridge, and the results obtained then were reliable.

6.2.3. Cracks

NPRA list the cracks on Cecilie Bridge as drying shrinkage and autogenous shrinkage cracks. According to the drawing, thermal dilatation could also be the reason, since the edge beam is casted later than the connected concrete. It was not possible to see a transition confirming different casting stages during the visual inspection under the bridge, the formwork seemed to be done in one piece.

6.3. Chloride ingress considering the impact of cracks

Core A from Cecilie Bridge shows the expected chloride ingress in accordance with Michel et al. (2013) (Figure 2.1). It indicates that chlorides were both detected on the surface and within the crack of core A. The chloride profile from the crack surface, seems to be so distinct that it is not reasonable to believe that it originated from somewhere else, for example chloride containing aggregates. The exception on the chloride ingress around the crack, was an area from 0.7 cm to 2.0 cm where there was no or very little chlorides detected. The chloride ingress from the crack surface from 0.0 cm to 0.7 cm have probably penetrated from the top surface. Meaning that the chloride ingress from the crack surface was from 2.0 cm and down. At the moment there is no explanation for this. But the chloride reducing coating mentioned in the drawing should be considered. And studies have shown that only parts of the surface of a crack filled with water, would act as a free surface for water sorption and chloride ion ingress (Pease 2010).

All the cores at Moholt show only chloride ingress from the top surface which is not very deep. It could not be stated that this ingress was deeper where at the cracks. It was no indication of any chloride ingress around the crack surface in cores from Moholt. They all showed the same information about chloride ingress, that it seems to be independent of crack and crack width. The chloride concentrations indicate a low exposure, and this might be a reason that it was hard to see obvious results. Core E from Moholt is a nice comparison to core A from Cecilie Bridge. They are quite similar in crack width and exposure, but show different chloride ingress.

Exposure time, crack width and average chloride ingress was a bit lower in core A at Cecilie Bridge, but still comparable to core E at Moholt Bridge. Core A from Cecilie Bridge showed a chloride ingress from the crack surface in addition to the chloride ingress from the top surface. This was a very different result than at Moholt Bridge, which only showed a chloride ingress from the top surface. Core E from Moholt Bridge had a larger crack width and higher observed chloride ingress from the surface compared to core A from Cecilie Bridge. Therefore, it could be expected that core E at Moholt Bridge should show the same or even higher ingress than core A at Cecilie Bridge (Audenaert et al. 2009). One observation regarding this was that water tends to rapidly drain off the edge beam at Moholt Bridge due to its curvature, and that the edge beam on Cecilie Bridge is flat, probably leaving water longer on the surface. Due to that a difference in exposure can be expected.

The fact that one bridge showed the expected results according to the expectations from laboratory experiments and the other bridge did not, proves that consideration is need before applying the laboratory research to real structures.

6.4. Reinforcement corrosion state in the cores

The draft note on “Carbonation of concrete cores from Moholt- and Ceciliebridge” should be read, since it contains the information on the reinforcement corrosion investigation. It is provided in Appendix F. The hand drawn description of the cores with detailed crack width, provided in Appendix E, could be useful information.

The highest chloride concentration observed in the cores was 0.36 element mass $\%_{xrf}$. This was in core E Moholt Bridge, located in the paste 8 mm bellow the top surface in an uncracked area. The core from Cecilie Bridge have similar concentration close to the top surface in the uncracked area, 0.33 element mass $\%_{xrf}$. Cecilie bridge is 16 years, versus Moholt Bridge’s 25 years, probably the load from chloride by year was higher at Cecilie Bridge**.** Critical chloride concentration at the reinforcement are given in Table 2.1. But there is an unknown difference between mass % and elemental mass $\%_{xrf}$.

According to the half-cell potential mapping and chloride ingress it was not expected any reinforcement corrosion due to chlorides. Although, when excavating the reinforcement in core E from Moholt Bridge, corrosion was discovered as shown in Figure 6.5.

Figure 6.5 Excavating the reinforcement from core E, Moholt Bridge

Mostly, the corrosion was found on the top half of the reinforcement where the crack originated. The bottom side and the reinforcement next by was only corroded to a little extent. The reason for corrosion could be carbonation. The typical half-cell potential range is different if carbonation is the reason for corrosion instead of chlorides. This is shown in Table 6.1.

Table 6.1 Typical range of HCP measured with $Cu/CuSO_4$ reference electrode. Based on RILEM TC 154-EMC. (Proceq 2016)

Properties of the concrete were the measured steel is embedded:	Typical range of HCP measured against a $Cu/CuSO_4$ reference electrode:
Water saturated concrete without O2	- 1000 to - 900 mV
Moist, chloride contaminated concrete	- 600 to - 400 mV
Moist, chloride free concrete	- 200 to + 100 mV
Moist, carbonated concrete	- 400 to + 100 mV
Dry, carbonated concrete	0 to + 200 mV
Dry, non-carbonated concrete	0 to + 200 mV

The core was easily split following the crack, by only using manual force. The crack surface and the area around the reinforcement was then sprayed with thymolphthalein. The crack surface was completely carbonated. Also, the concrete surface connected to the corroding part of the reinforcement was carbonated. The crack surface on the core from Cecilie Bridge was tested in the same way, it showed the same results as core E from Moholt Bridge regarding carbonation on the crack surface. The Cecilie Bridge core did not contain reinforcement.

In moist climate, like in Trondheim, it was not expected carbonation in a crack, since water limit carbonation due to lack of air containing CO_2 (Herholdt et al. 1979). This can be related to the water draining of the edge beam.

7. Conclusion

The purpose of this project was to do a field study to investigate a relation between cracks and deeper chloride ingress and possible corrosion initiation. Two bridges in Trondheim, Moholt Bridge and Cecilie Bridge were investigated.

First was half-cell potential mapping done at Moholt Bridge to locate points of interest and the results indicated that there probably was no active corrosion due to chlorides. Three cores were drilled to further examine this. The cores had quite comparable properties, and crack width was the varying factor.

From µ-XRF scans of the cores from Moholt Bridge, no difference in chloride ingress was observed between the core with 0.55 mm crack width, 0.15 mm crack width and the reference core with no crack. They all showed a similar chloride ingress, evenly distanced from the top surface and no additional chloride ingress at the crack surface. The chloride ingress was overall very small, indicating limited exposure.

After that, one core was drilled at Cecilie Bridge and investigated. This core had a crack width of 0.45 mm. The core from Cecilie Bridge showed a chloride ingress both from the top surface and the crack surface. This is according to expectations from laboratory experiments on the topic, namely a deeper ingress around cracks. A potential explanation for the different results is that due to the slope on the edge beam at Moholt Bridge, water tend to drain off rapidly. While Cecilie Bridge is horizontal, probably leaving water longer on the surface.

Moholt Bridge and Cecilie Bridge are quite similar constructions, but showed opposite results on chloride ingress through cracks. This illustrates the importance of field studies and that consideration need to be taken before applying laboratory results on real structures.

For further investigations on the potential impact of cracks, it might be efficient to initially extract a few cores as background for planning of more detailed investigation. This method was used on Cecilie Bridge, and proved to work well.

Corrosion was detected in core E from Moholt Bridge, on the reinforcement closest to the crack. There was not detected any chlorides in the crack, but the crack surface was completely carbonated. Also, the concrete surface connected to the corroding part of the reinforcement was carbonated. This could indicate carbonation as the cause for the observed corrosion. The different expectation from corrosion due to carbonation and chlorides could explain why the half-cell potential mapping gave a low probability of corrosion.

8. Future investigation

The examined edge beam both on Moholt Bridge and Cecilie Bridge lacked sufficient exposure to obtain obvious results on chloride ingress. For future investigation, it is recommended to investigate an edge beam closer to the driving lanes, where most de-icing salt is used.

Drilling a core from Cecilie Bridge including reinforcement is recommended. The crack surface was carbonated in the core from Cecilie Bridge, but the impact on reinforcement corrosion was not checked for this bridge.

9. Reference list

Angst, U. Elsener, B. Larsen, C.K. Vennesland, Ø. (2009) “Critical chloride content in reinforced concrete – A review”, Cement and Concrete Research, Volume 39, December 2009, pp 1122-1138

Audenaert, K. De Schutter, G. Marsavina, L. (2009) “Influence of cracks and crack width on penetration depth of chlorides in concrete", European journal of environmental and civil engineering, 13(5), pp 561-572

ASTM 876-15 (2015) "Standard Test Method for Corrosion Potentials of Uncoated Reinforcing Steel in Concrete"

Beeby, A. W. (1978) “Concrete in the oceans; cracking and corrosion”, Wexham Springs

Bjontegaard, Ø. 09.03.2017, Personal communication and lecture

Bjontegaard, Ø. (2009) “Shrinkage, cracking”, in Jacobsen, S. Concrete Technology, Chapter 13, Trondheim 2016

Danner, T (2017) Personal communication and email

Danner, T. De Weerdt, K. Geiker, M. R. (2017) “µ-XRF – Characterisation of Chloride Ingress and Self-healing in Cracked Concrete”, submitted to XXIIIth Symposium on Nordic Concrete Research & development, Aalborg, Denmark, August 2017

Edvardsen, C. (1999) “Water permeability and autogenous healing of cracks in concrete”, Aci Materials Journal, 96, pp 448-454

Eklima (2017) Available at: http://sharki.oslo.dnmi.no/pls/portal/BATCH_ORDER.RPT_BATCH_STORE.show (accessed 24 April 2017)

Environmental package (2017) Avaliable at: http://miljopakken.no/wp-content/uploads/2016/01/Vinterdrift-16-17.pdf (accessed 24 April 2017)

Elsener, B. Andrade, C. Gulikers, J. Polder, R. Raupach, M. (2003) “Half cell potential measurements – Potential mapping on reinforced concrete structures”, Rilem TC 154-EMC, Materials and structures, vol 36, pp 603-611

Elsener, B. and Bohni, H. (1997) "Half-cell potential measurements - From theory to condition assessment of RC structures", Proc. Int. Conference "Understanding Corrosion Mechanisms of Metals in Concrete - A Key to improving Infrastructure Durability", Massachusetts Institute of Technology, MIT (Cambridge, USA), 27-31 July 1997, Keynote lecture session No. 3.

Elsener, B. and Bohni, H. (1990) “Potential Mapping and Corrosion of Steel in Concrete”, Corrosion rates of Steel in concrete, ASTM STP 1065, Berke, N.S. et al, American Society for Testing and Materials, Philadelphia, 1990, pp 143-156

Geiker, M. R. (2017) Personal communication

Geiker, M. R. (2012) “Reinforcement corrosion”, in Jacobsen, S. Concrete Technology, Chapter 16, Trondheim 2016

Geiker, M. R. and Michel, A. (2017) “Half cell Potential measurements of reinforced concrete”, DTU Course 11569 Durability and repair of concrete structures, DTU, January 2017

Herholdt, Aa. D. Justesen, C. F. P. Nepper-Christensen, P. Nielsen, A (1979) “Beton-Bogen”, Cementfabrikkernes tekniske oplysningskontor, Aalborg portland

Hornbostel K, Larsen, C K. Geiker, M R. (2013) “Relationship between concrete and corrosion rate – A literature review”, Cement & Concrete Composites, 39, pp 60-72

Hornbostel, K. and Geiker, M. (2016) “Note on influence of cracks on corrosion”, Internal document at NTNU

Hornbostel K. (2016) Personal communication 01.12.2016

Lindquist, W D. Darwin, D. Browning, J. Miller, G G. (2006) “Effect of Cracking on Chloride Content in Concrete Bridge”, ACI Matherials Journal, Title no. 103-M52

Michel, A. Solgaard, A.O.S. Pease, B.J. Geiker, M.R. Stang, H. Olesen, J.F. (2013), “Experimental investigation of the relation between damage at the concrete-steel interface and initiation of reinforcement corrosion in plain and fibre reinforced concrete", Corrosion Science, volume 77, December 2013, pp 308-321

Minnoreti A. (2017) 06.04.2017 E-mail

Moradllo, M. K. Sudbrink, B. Qinang, H. Aboustait, M. Tabb, B. Ley, M. T. Davis, J. M. (2017) "Using micro X-ray fluorescence to image chloride profiles in concrete", Cement and Concrete Research, 2017, 92, pp 128-141

M4 Tornado Manual (2015) "M4 Tornado – High performance micro-XRF spectrometer", Bruker Nano GmbH, Berlin, Germany

Norwegian Public Roads Administration (1997) “15.516 Utboring av kjerner”, in Håndbok R211 Feltundersøkelser

Norwegian Public Roads Administration (1997) “15.551 Armeringens elektrokjemiske potensiale", in Håndbok R211 Feltundersøkelser

Otieno, M. B. Alexander, M. G. Beushausen, H. D. (2010) "Corrosion in cracked and uncracked concrete - influence of crack width, concrete quality and crack reopening.", Magazine of Concrete Research, 62, pp 393-404.

Pease, B. (2010) “Influence of concrete cracking on ingress and reinforcement corrosion"

Polder, R. Andrade, C. Elsener, B. Vennesland, Ø. Gulikers, J. Weidert, R. Raupach, M. (2000) “Test methods for on site measurement of resistivity of concrete”, Rilem TC 154-EMC, Materials and structures, vol 33, pp 603-611

Poulsen, E. et al. (1985) “13 betonsygdomme – Hvordan de opstår, forløber og forebygges (13 Concrete deseases- How they occour, pass and could be prevented)”, Beton 4, SBI, pp 82-83, Hørsholm 1985

Proceq SA (2016) “Profometer Operating Instructions”

Rodum, E. (2010) “Alkalireaksjoner i betong – hvordan håndterer vi dette?" Available at: http://docplayer.me/19976895-Alkalireaksjoner-i-betong-hvordan-handterer-vi-dette.html (accessed 30 March 2017)

Savija, B. and E. Schlangen, (2016) *Autogenous healing and chloride ingress in cracked concrete.* Heron, 2016. 61(1): p. 15-32

Skare, E. Stemland, K. (2015) “Kartlegging av rissdannelse i broer”, Project report NTNU

Strømme, Ø. (2017) “Influence of concrete imperfections on chloride penetration and reinforcement corrosion”, Master thesis, NTNU 2017

Vegvesen a (2017) Available at: http://www.vegvesen.no/fag/veg+og+gate/Drift+og+vedlikehold/Vinterdrift/standardkrav (accessed 24 April 2017)

Vegvesen b (2017) Available at: https://www.vegvesen.no/vegkart/vegkart/#kartlag:geodata/hva:(~(id:810,filter:(~),farge:%270_0))/@272584,7039269,16/vegobjekt:571325318:58b02c (accessed 24 April 2017)

Vegvesen c (2017) Available at: https://www.vegvesen.no/vegkart/vegkart/#kartlag:geodata/hva:(~(id:810,filter:(~),farge:%270_0))/@272584,7039269,16/vegobjekt:573271958:58b02c (accessed 24 April 2017)

10. Appendix

10.1. Appendix A - Construction drawing of Moholt Bridge

Figure 10.1 – 10.4 show construction drawings of Moholt Bridge

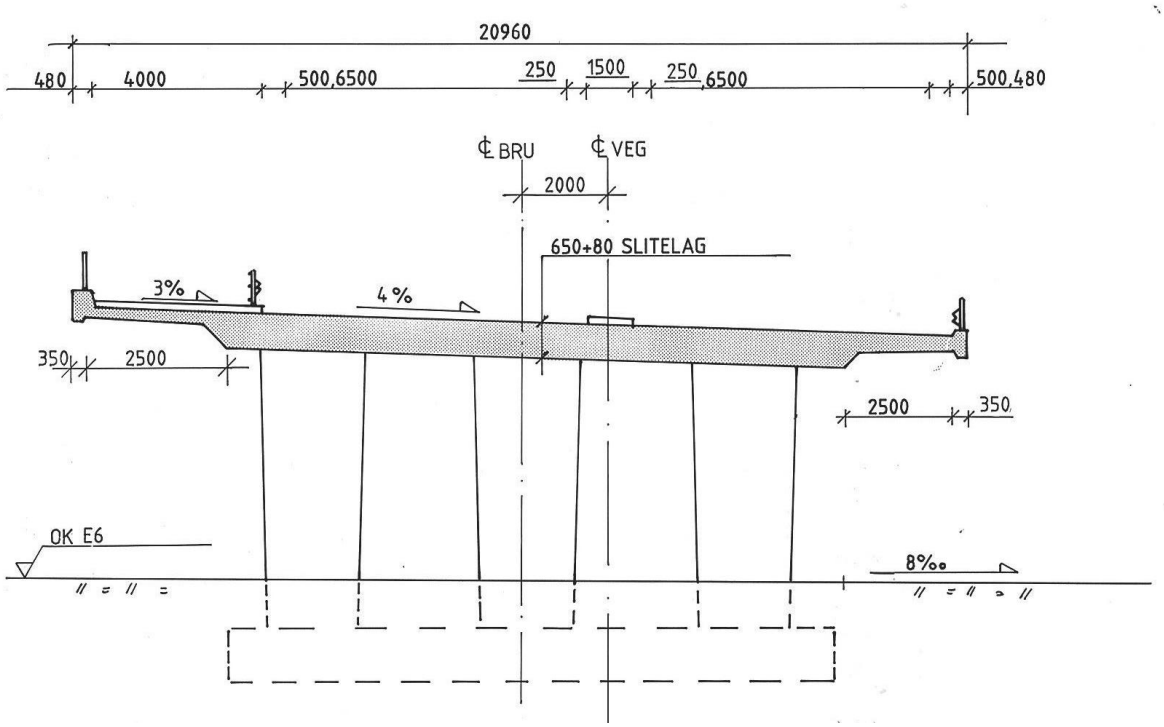

Figure 10.1 Drawing Moholt Bridge 1

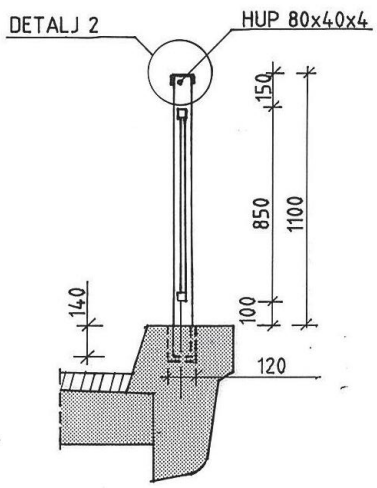

GÅNGBANEREKKVERK

Figure 10.2 Drawing Moholt Bridge 2

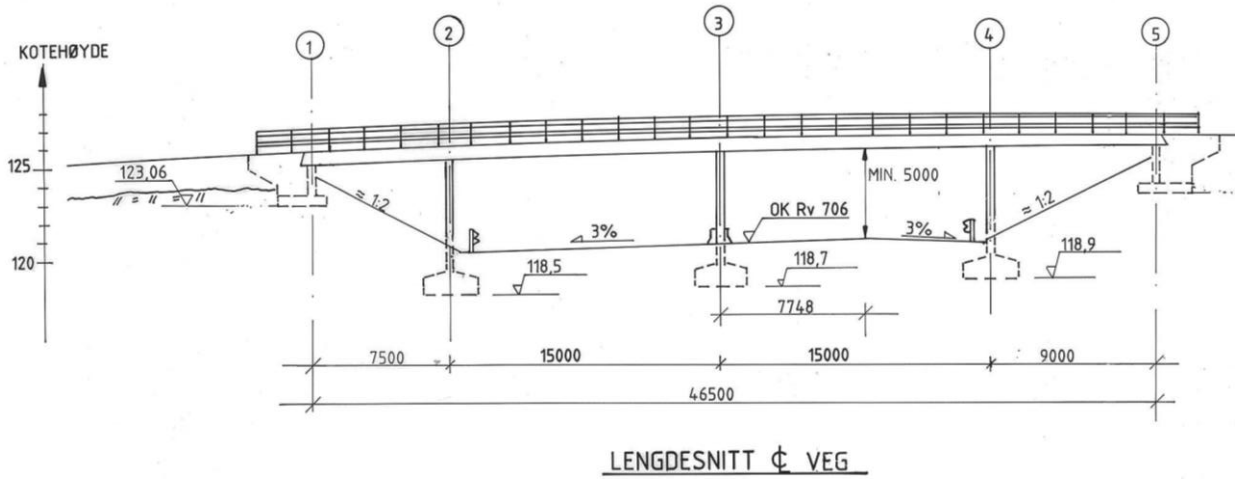

Figure 10.3 Drawing Moholt Bridge 3

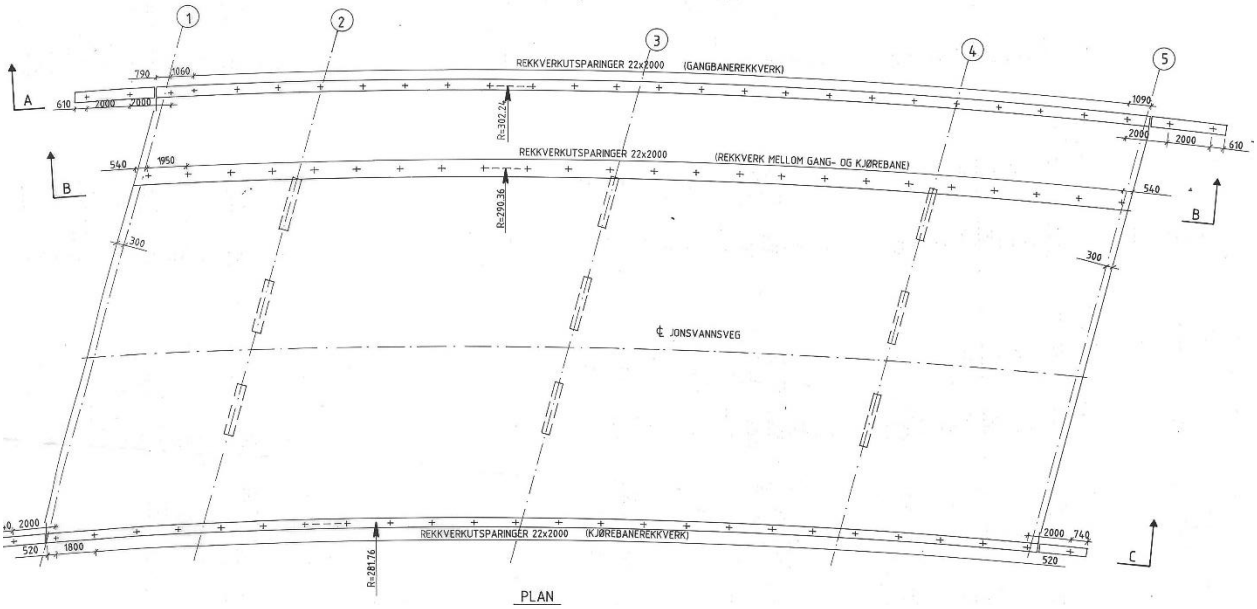

Figure 10.4 Drawing Moholt Bridge 4

10.2. Appendix B - Weather data at Moholt Bridge

Figure 10.5 show weather log from Moholt Bridge. Figure 10.6 show background data for the wind rose in Figure 3.3

Trondheim (Voll) målestasjon Stasjonen ligger i Trondheim kommune, 127 m o.h. Den er nærmeste offisielle målestasjon, 0,0 km fra punktet Trondheim (Voll) målestasjon. Stasjonen ble opprettet i januar 1923. Stasjonen måler nedbør, temperatur, snødybde og vind. Det kan mangle data i observasjonsperioden.

Tabell for temperatur, nedbør og vind per dag

Dato	Temperatur °C				Nedbør			Vind i m/s	
	Maks	Min	Middel	Normal	Akkumulert nedbør i mm (målt kl 7 for siste 24 timer)	Nedbørtype	Snødybde cm	Maks	Middel
28. februar 2017	5,3°	-2,1°	1,9°	-1,5°	0,9 mm	---	2 cm	4,5 m/s	2,7 m/s
27. februar 2017	4,8°	-2,4°	0,7°	-1,6°	1,5 mm	---	10 cm	4,3 m/s	1,3 m/s
26. februar 2017	3,3°	-2,9°	0,6°	-1,7°	3,3 mm	---	10 cm	3,9 m/s	1,6 m/s
25. februar 2017	-0,9°	-6,0°	-2,7°	-1,8°	5,1 mm	---	10 cm	3,7 m/s	1,9 m/s
24. februar 2017	-1,2°	-4,0°	-2,7°	-1,9°	3,9 mm	---	5 cm	5,0 m/s	2,3 m/s
23. februar 2017	-0,1°	-3,9°	-2,5°	-2,0°	6,2 mm	---	---	5,9 m/s	3,1 m/s
22. februar 2017	1,8°	-3,8°	0,2°	-2,1°	1,0 mm	---	---	4,8 m/s	2,6 m/s
21. februar 2017	2,7°	-3,6°	-2,2°	-2,2°	1,5 mm	---	0 cm	---	1,0 m/s
20. februar 2017	1,3°	-1,7°	-0,6°	-2,3°	13,6 mm	---	---	---	---
19. februar 2017	6,6°	1,3°	3,9°	-2,3°	10,1 mm	---	0 cm	9,5 m/s	4,2 m/s
18. februar 2017	6,3°	1,8°	4,4°	-2,4°	5,2 mm	---	0 cm	5,0 m/s	3,2 m/s
17. februar 2017	4,8°	2,3°	3,3°	-2,5°	4,3 mm	---	0 cm	5,6 m/s	3,6 m/s
16. februar 2017	4,3°	0,1°	2,1°	-2,6°	1,6 mm	---	0 cm	3,7 m/s	2,1 m/s
15. februar 2017	3,6°	-4,1°	-0,7°	-2,6°	0,4 mm	---	0 cm	3,6 m/s	1,2 m/s
14. februar 2017	5,1°	2,4°	2,9°	-2,7°	0,0 mm	---	0 cm	3,3 m/s	1,8 m/s
13. februar 2017	5,4°	1,6°	4,5°	-2,8°	0,0 mm	---	0 cm	4,7 m/s	3,2 m/s
12. februar 2017	2,3°	-8,3°	-2,9°	-2,8°	0,7 mm	---	0 cm	4,7 m/s	3,0 m/s
11. februar 2017	-0,4°	-6,1°	-4,1°	-2,9°	0,1 mm	---	0 cm	3,2 m/s	1,6 m/s
10. februar 2017	-1,1°	-6,9°	-3,2°	-2,9°	1,0 mm	---	0 cm	3,7 m/s	1,7 m/s
9. februar 2017	-0,3°	-10,3°	-4,7°	-2,9°	0,1 mm	---	0 cm	4,0 m/s	1,3 m/s
8. februar 2017	-4,0°	-10,1°	-7,6°	-3,0°	0,2 mm	---	0 cm	6,4 m/s	1,9 m/s
7. februar 2017	0,1°	-6,6°	-5,1°	-3,0°	0,1 mm	---	---	7,8 m/s	3,2 m/s
6. februar 2017	3,7°	-0,7°	1,3°	-3,0°	0,5 mm	---	0 cm	6,6 m/s	3,8 m/s
5. februar 2017	2,5°	-1,5°	0,9°	-3,1°	0,7 mm	---	0 cm	5,1 m/s	2,2 m/s
4. februar 2017	2,4°	-5,8°	-1,8°	-3,1°	0,3 mm	---	0 cm	4,9 m/s	2,1 m/s
3. februar 2017	1,3°	-3,1°	-1,5°	-3,1°	0,6 mm	---	0 cm	3,2 m/s	1,4 m/s

Figure 10.5 Weather data covering the periode when all the measurments where done at Moholt Bridge

Frequency distribution - wind rose

Norwegian Meteorological Institute

Stations

Stnr	Name	Operates from	Operates until	Altitude	Latitude	Longitude	Municipality	County	Region
68860	TRONDHEIM - VOLL	Jan 1923		127	63,4107	10,4538	Trondheim	Sør-Trøndelag	TRØNDELAG

Elements

Code	Name	Unit
DD	Wind direction (FF)	degrees
FF	Wind speed (10 meters above ground)	m/s

Norwegian Mean Time (NMT) is the same as Central European Time which is the timezone one hour before UTC, and is therefore oft described by UTC+1. It does not change in summer. NMT gives the hours from 01 to 24.

*** NOTE ***

In the period 01.01.1992 - 28.02.2006 data from the synoptic main observations are used for FF and DD.

68860 Relative frequencies (%) of observations grouped by DD horizontally and FF vertically. 01.01.1992 - 28.02.2006

Jan, Feb, Mar, Apr, Nov, Dec. All available hours

	DD	345	15	45	75	105	135	165	195	225	255	285	315	Variable	Calm	Total	Rel.fr.	Cum.fr.	Mean	St.dev.
FF		14	44	74	104	134	164	194	224	254	284	314	344						DD	DD
<=	0,2														3,7	338	3,7	3,7		
0,3	5,2	1,9	5,2	5,9	4,5	2,6	3,2	17,0	28,5	10,1	3,3	2,6	1,8			7884	86,5	90,2		
5,3	10,2	0,0	0,0	0,0				3,6	1,4	2,4	1,1	0,4	0,1			840	9,2	99,4		
10,3	15,2							0,1		0,4	0,0					52	0,6	100,0		
15,3	20,2																			
>	20,2																			
Total		176	478	539	412	233	295	1884	2723	1181	412	273	170		338	9114				
Rel.fr.		1,9	5,2	5,9	4,5	2,6	3,2	20,7	29,9	13,0	4,5	3,0	1,9		3,7		100,0			
Cum.fr.		1,9	7,2	13,1	17,6	20,2	23,4	44,1	74,0	86,9	91,4	94,4	96,3		100,0					
Mean	FF	1,8	2,0	1,8	1,9	1,8	1,8	3,8	2,8	3,9	3,9	3,3	2,5		0,0					
St.dev.	FF	1,1	1,0	1,0	1,0	0,9	1,1	2,0	1,4	2,5	2,5	1,9	1,6		0,0					

Statistics

Statistics	FF	DD	Date
Mean	2,9		
St.dev.	2,0		
Min FF	0,0		01.01.2002 19:00
Max FF	13,4		04.12.2003 07:00
Min DD			
Max DD			
Data coverage	15%	15%	

Time of observations are given in Norwegian Mean Time (NMT=UTC+1)

Figure 10.6 Background data for the wind rose in Figure 3.3

10.3. Appendix C - More in detail measurements from Moholt Bridge

Figure 10.7 show all HCP data from Moholt Bridge togheter.

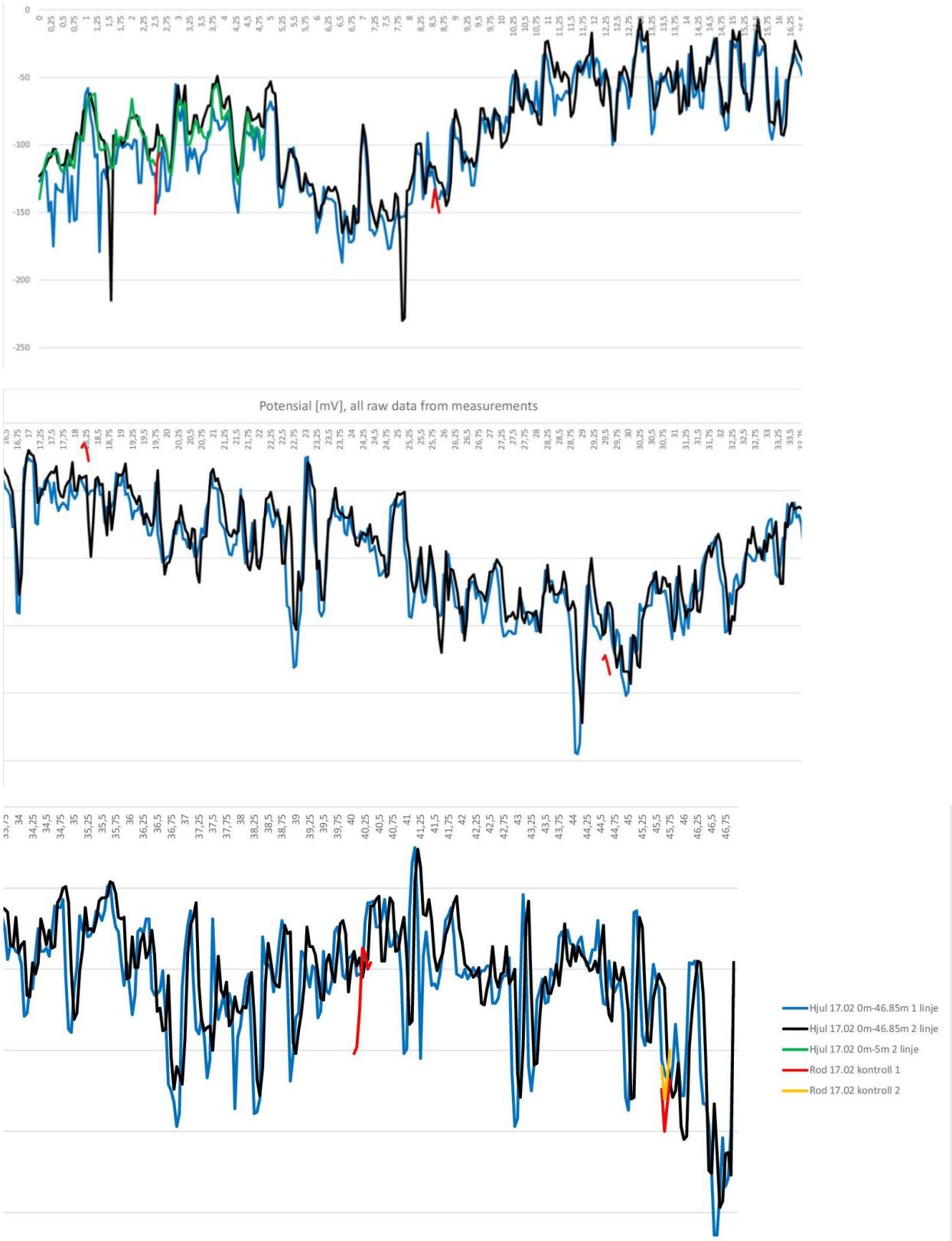

Figure 10.7 All the potential measurements at Moholt Bridge plotted togehter on the same x-axis from 0.0 m on the east and to 46.85 meters on the west end.

Figure 10.8 and 10.9 shows HCP data in the *Profometer* software.

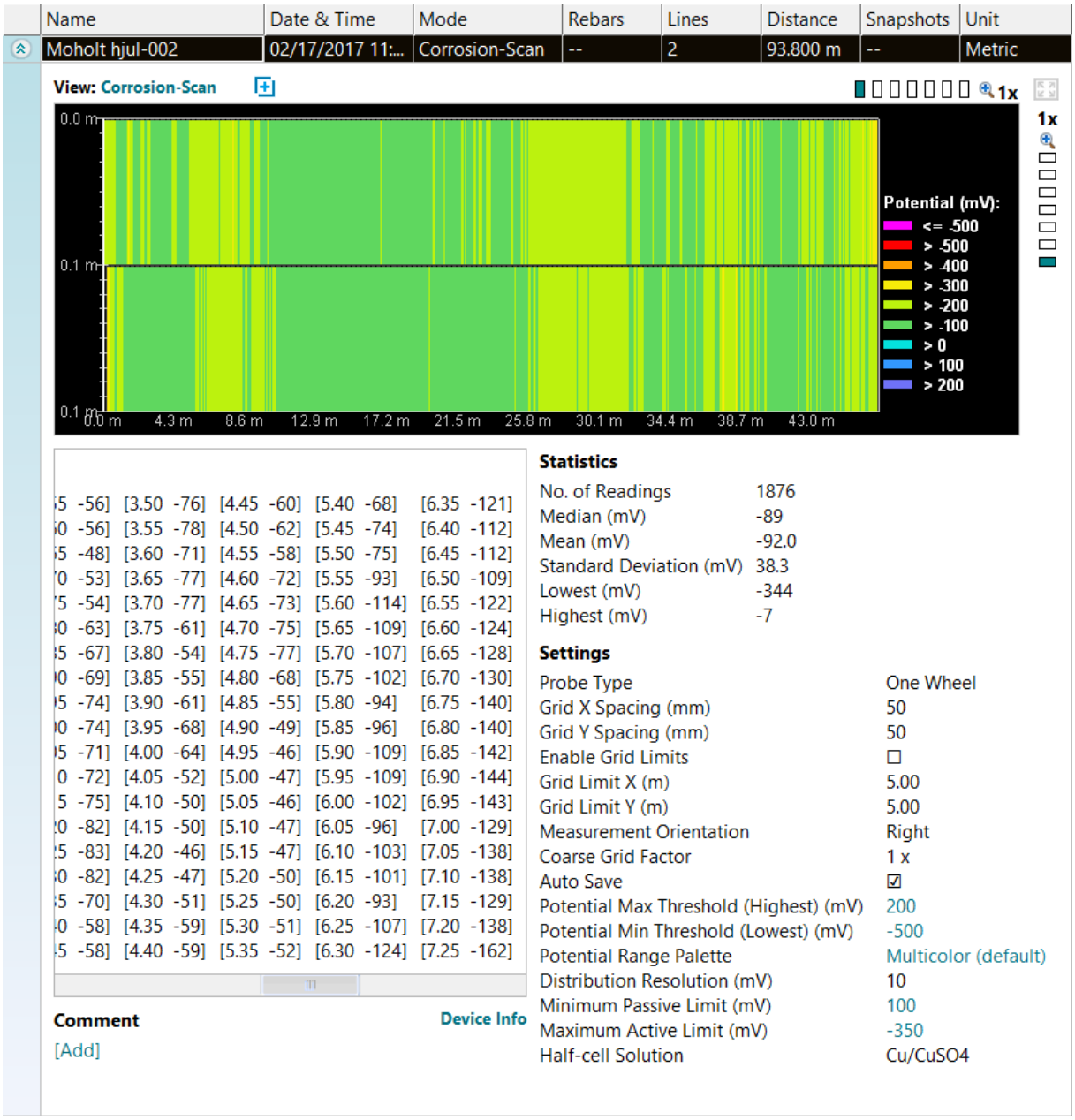

Figure 10.8 The half-cell potential data as shown in the Profometer software. This is the values repsented as "Hjul 17.02 0m-46.85m 2 linje" in Figure 10.7

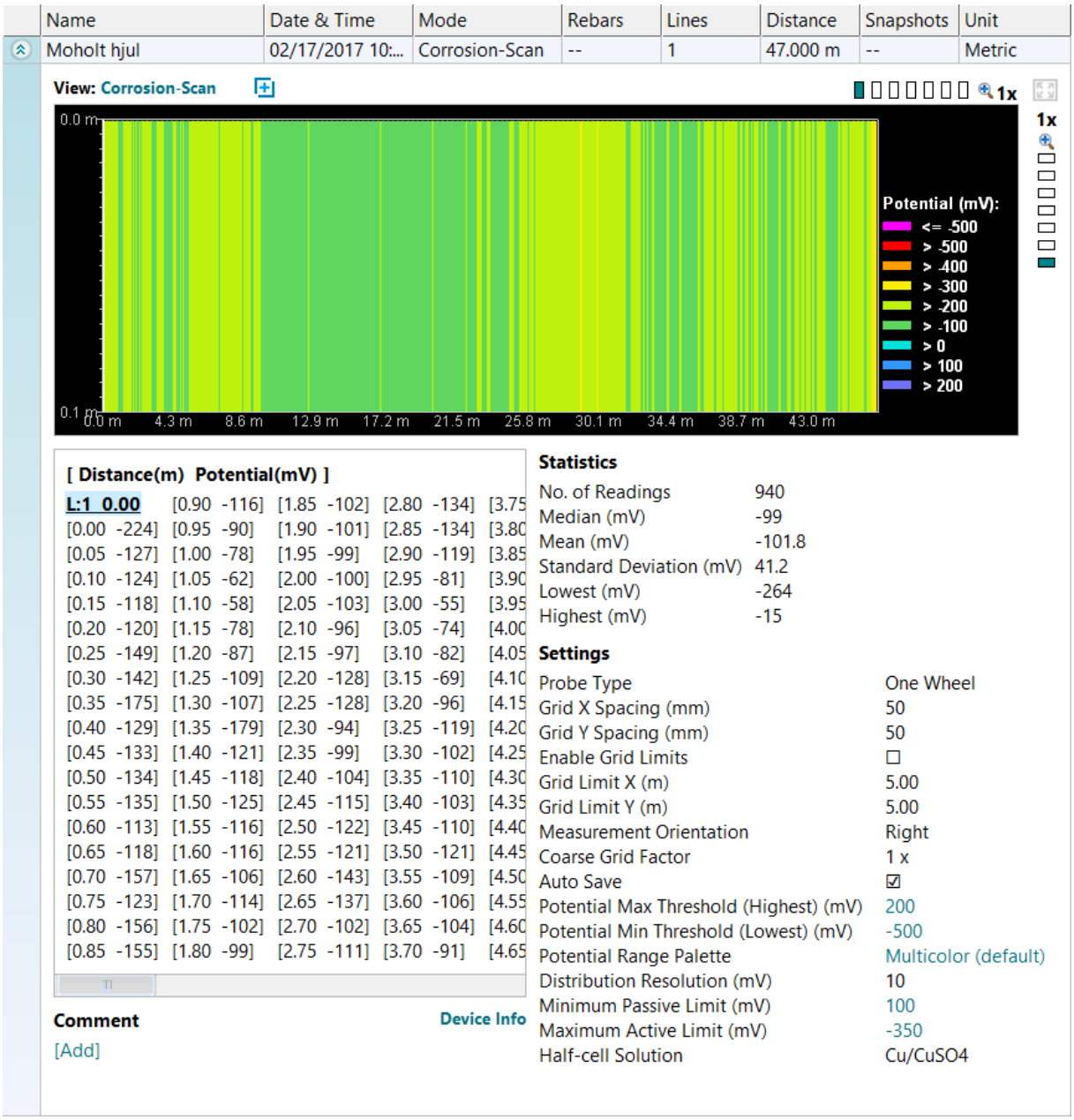

Figure 10.9 The half-cell potential data as shown in the profometer software. This is the values repsented as "Hjul 17.02 0m-46.85m 1 linje" in Figure 10.7

Resistivity measurement 17.02.2017

Distance [m]	Point 1 [kΩcm]	Point 2 [kΩcm]	Comments:
0,75	15,6	16	
1,65	18,9	25,1	
2,25	24	22,8	
3,6	15,1	23,2	
4,2	20,2	18,6	
5,35	15,5	17,1	
6,5	15,2	20,5	
7,45	19,1	18,4	
8,45	16,7	21,1	
9,8	21,5	24,8	
10,55	16	17	
11,5	20,5	19,9	
12,4	18,5	20,5	
13,6	20,5	22,6	
14,55	9,9	22,5	Narrow
16,2	21	19,8	
17,65	22	21,1	
18,55	17,4	21,3	Narrow
20,1	15	13,9	Narrow
21,7	16,4	14,7	
22,6	13,3	11,2	Narrow
24,1	12,1	10,5	
25,35	13,6	11	
26,55	12,1	13	
27,9	7,8	8,3	
29,5	5,9	7,8	Low cover depth
30,3	11,1	10,7	
31,45	11,2	11,6	
31,8	12,5	16,5	
32,4	7,3	8,5	Narrow
33,7	16,5	17	
34,8	13,5	15	Narrow
35,6	17,1	17,5	
36,6	13,4	17,6	
37,5	15,5		
38,65	11,3	15,5	
39,8	14,3	16	
40,15	17	18,7	
41,45	15	14,3	
42,1	14,6	10	
43,45	11,7	15,4	
44,45	15,2	15,5	
45,4	18	18,3	
46,5	16,9	18,3	
Average	15,4	16,7	

Point 1:
Closest to the pedestrian lane

Point 2:
Away from pedestrian lane,
other side of the fence

10.4. Appendix D - Overview of different crack types

This is a more in detail overview of different crack mechanisms. It should be known that the fresh phase is the first hours, from mixing trough casting and till the concrete starts to set and get strength. Then the hardening phase last for a week or two, until the reactions is so slow that we start calling it the service phase. This and the following overview of different crack mechanisms, focus on factors indicating time of development and expectations for width changes, and is based on Bjontegaard (2009). Table 10.1 and Figure 10.10 show an overview of different cracks.

10.4.1. Plastic settlement

In the fresh phase particles sink down, and water and air voids may move upwards. Settlement in concrete is often 0.5 – 1.0 %. Different conditions for settlement in casted concrete could lead to forming of cracks. Cracks will be formed over the reinforcement if it prevents the setting. Or where the cross-section changes from low to higher, because there will be more settlement in high cross-sections.

10.4.2. Autogenous shrinkage

The chemical reaction between water and cement is the background for autogenous shrinkage. Because the volume of the product is lower than the initial volume of each of them separate. Contraction forces because of the meniscus and under pressure in the pores, comparable to plastic shrinkage and drying shrinkage, will emerge. This inner contraction forces will reduce the concrete volume in all directions, isotropic. The outer result of this is autogenous shrinkage, which could lead to cracks in the concrete. It can take months before cracks are formed in the concrete.

10.4.3. Drying shrinkage

Over time the concrete will dry on surfaces that are exposed to air. It is the same prosses as in plastic shrinkage, where negative pore pressure is the driving force, but now we talk about the time after the concrete is hardened. The concrete will first retract on the surface, because it takes time before the drying spread inward of the cross section. This will be a reason for cracks on the surface. Especially if the drying is only on one surface, the contraction difference through the cross section varies a lot. The crack pattern from drying shrinkage could be a random map cracking or it could follow the reinforcement.

10.4.4. Plastic shrinkage

Plastic shrinkage happens in the fresh phase of concrete. And experience shows that cracks develop as soon as 15 minutes to 8 hours after casting. It will only happen on horizontal surfaces where there is no protection for exposure to the environment. Other surfaces will be protected by the formwork. What happens is that the surface lose water to the air faster than the concrete transport new water to the surface, when the surface then is dry, the concrete contracts. Warm weather, especially sunshine, and wind will facilitate the effect because evaporation of water is heightened under those conditions. The contraction occurs because a capillary force will drag the particles closer to each other when the water surface is so low that it forms a meniscus between the particles. Cracks caused by plastic shrinkage are wide and deep, although it is conditions on the surface who form them. They could often go deeper than the first layer of reinforcement. They are often drop-shaped, meaning that

they are even wider a little bit down in the concrete then we can measure on the surface. Typical a random crack pattern. (Bjontegaard 2017)

10.4.5. Thermal dilation/contraction

Stresses because of temperature differences in the fresh and hardening phase. Concrete temperature raises during the chemical reactions, which are fastest in the beginning. Heat will build up in the structure, especially in thick cross sections during warm weather, because the heat generation is higher than heat loss to the environment. The underlaying principle is expansion from heat and contraction from cold. The cracks may form due to the stresses that develop when the temperature start to fall again, due to either internal or external restraint. Internal restraint is when the surface cool down and contract before the core. But that tends to fix itself given some time to even out the temperature so that the contraction becomes equal through the cross section.

External restraint is worse in the case of cracking. That happens when concretes are casted in connection with each other, but not at the same time. Then the old concrete would not have the same temperature rise as the fresh concrete. Meaning that it wouldn't have the same potential to cool down and contract. So, when the fresh concrete cool down and contract, the old concrete would not. Therefor it would be a constant restraint and eventual cracks from the contraction in the fresh concrete, would not fix them self over time. That kind of cracks tend to be so deep that they go through the whole cross section. They are focused close to where the restraint is and the direction will be away from the restraint. The cooling down of normal concrete structures will be during the hardening phase, so that is when the cracks will develop.

10.4.6. ASR

Alkali-Silica Reactions (ASR) is a chemical reaction between some type of aggregates and the alkaline in the paste. The gel that then form will take up water and swell, this volume increase may form cracks. Typical reactive aggregates in Norway tend to react slow, it takes usually 15-20 years before it shows in the concrete. (Rodum 2010)

10.4.7. Degradation

When the reinforcement corrodes, it expands. This expansion generates stresses and possibly damages in the concrete.

Water expands about 9 % when it freezes. Liquid water fill pores or cracks, and when it freezes the expands could break loose part of the concrete, or widen the cracks. This degradation mechanism is called freeze-thaw.

Combinations of these are common, for example: ASR make a crack, freeze-thaw widens it, chlorides penetrate and start early corrosion.

10.4.8. Loading

Loading will cause strain and compression on a cross section. On the strain side cracks develop or amplify. On the compression side, cracks are reduced.

Table 10.1 Overview of different cracks, the letters refers to Figure 10.10

Type of cracking	Position on Fig. 3.3	Subdivision	Most common location	Primary cause (excluding restraint)	Secondary causes/ factors	Remedy (assuming basic redesign is impossible). In all cases reduce restraint	For further details see section ...	Time of appearance
Plastic settlement	A	Over reinforcement	Deep sections	Excess bleeding	Rapid early drying conditions	Reduce bleeding (air entrainment) or revibrate	3.1	10 minutes to 3 hours
	B	Arching	Top of columns					
	C	Change of depth	Trough and waffle slabs					
Plastic shrinkage	D	Diagonal	Roads and slabs	Rapid early drying	Low rate of bleeding	Improve early curing	3.1	30 minutes to 6 hours
	E	Random	Reinforced concrete slabs					
	F	Over reinforcement	Reinforced concrete slabs	Rapid early drying, steel near surface				
Early thermal contraction	G	External restraint	Thick walls	Excess heat generation	Rapid cooling	Reduce heat and/or insulate	3.1 Appendix 1	1 day to 2–3 weeks
	H	Internal restraint	Thick slabs	Excess temperature gradients				
Long-term drying shrinkage	I		Thin slabs (and walls)	Inefficient joints	Excess shrinkage, inefficient curing	Reduce water content, improve curing	3.1	Several weeks or months
Crazing	J	Against formwork	'Fair-faced' concrete	Impermeable formwork	Rich mixes	Improve curing and finishing	3.1	1–7 days, sometimes much later
	K	Floated concrete	Slabs	Over-trowelling	Poor curing			
Corrosion of reinforcement	L	Natural	Columns and beams	Lack of cover	Poor quality concrete	Eliminate causes listed	6.2	More than 2 years
	M	Calcium chloride	Precast concrete	Excess calcium chloride				
Alkali-aggregate reaction	N		(Damp locations)	Reactive aggregate plus high-alkali cement		Eliminate causes listed	4.4	More than 5 years

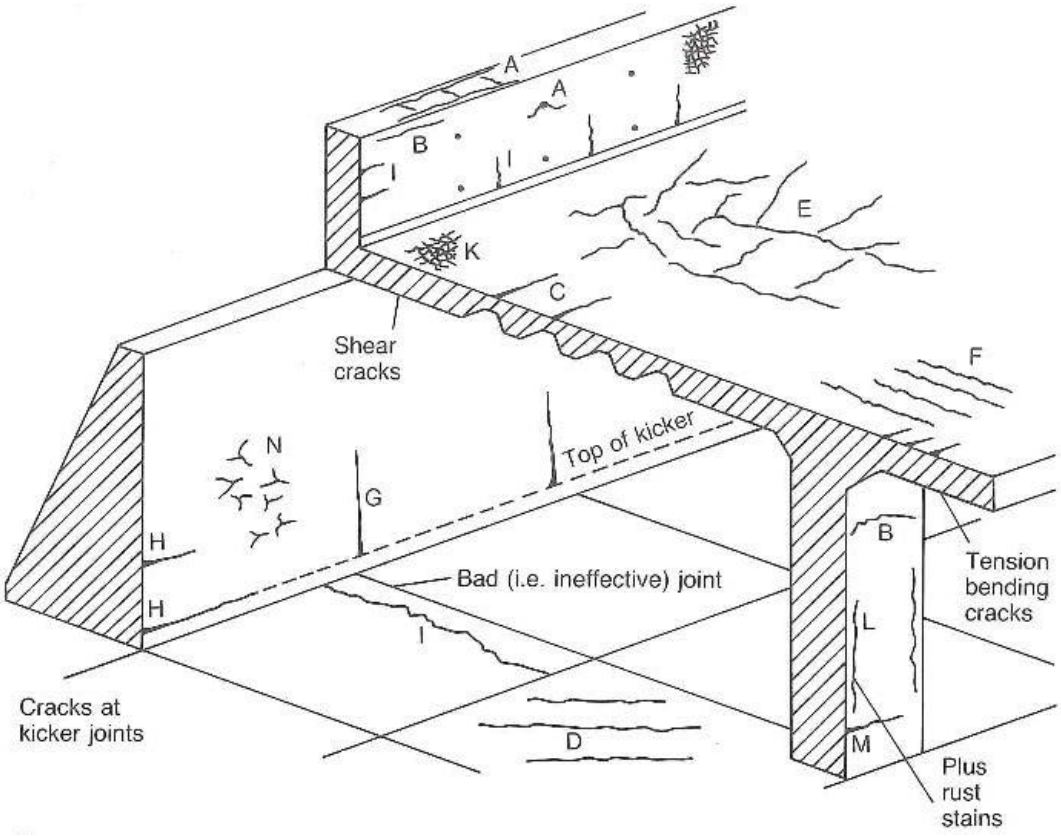

Figure 10.10 Picture describing different cracks on a structure, letters reffer to Table 10.1

10.5. Appendix E – Details on the cores from Moholt Bridge

Figure 10.11 – 10.14 show point of interest and detailed crack width of cores from Moholt.

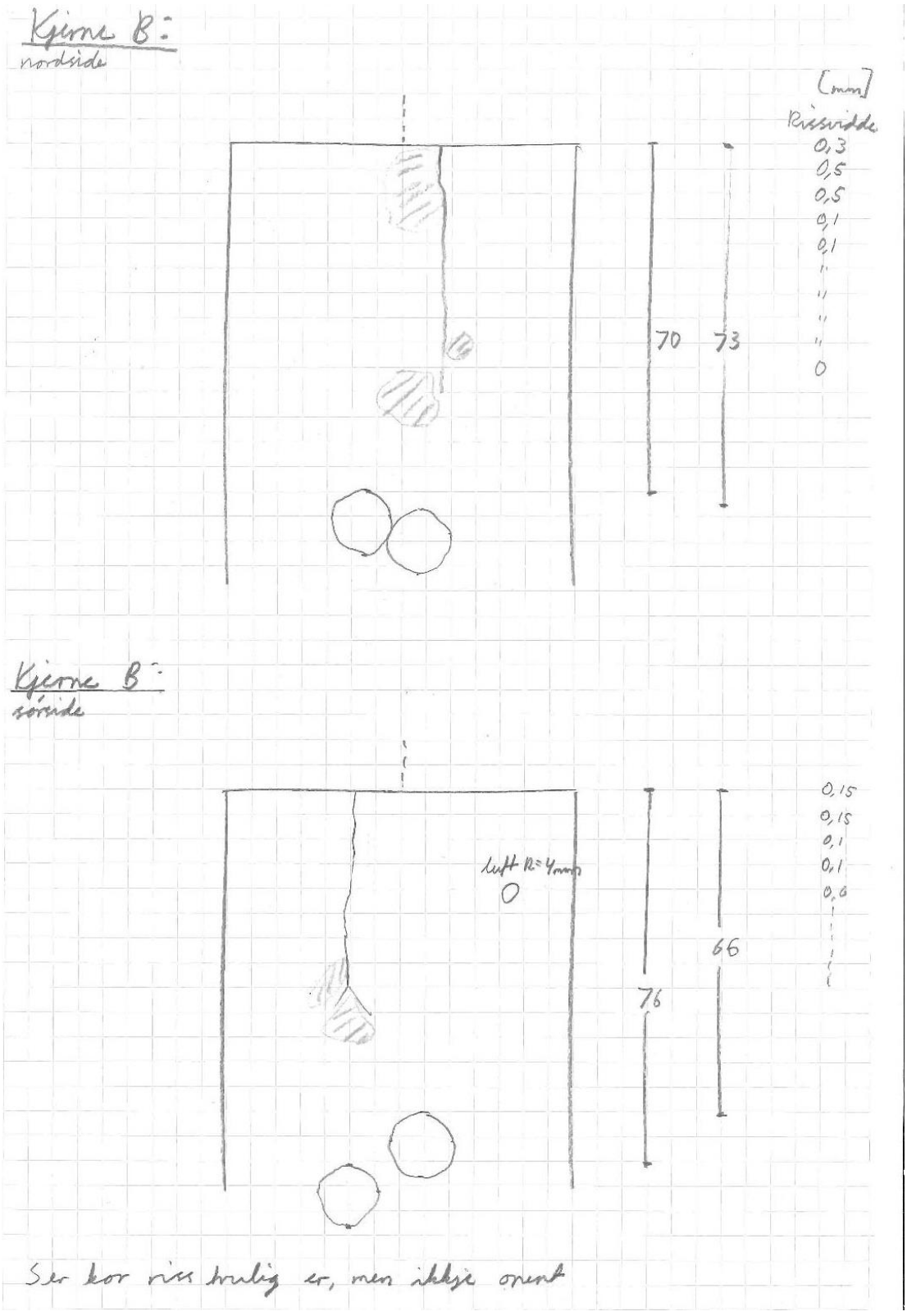

Figure 10.11 Drawing of core B with point of interest and detailed crack width.

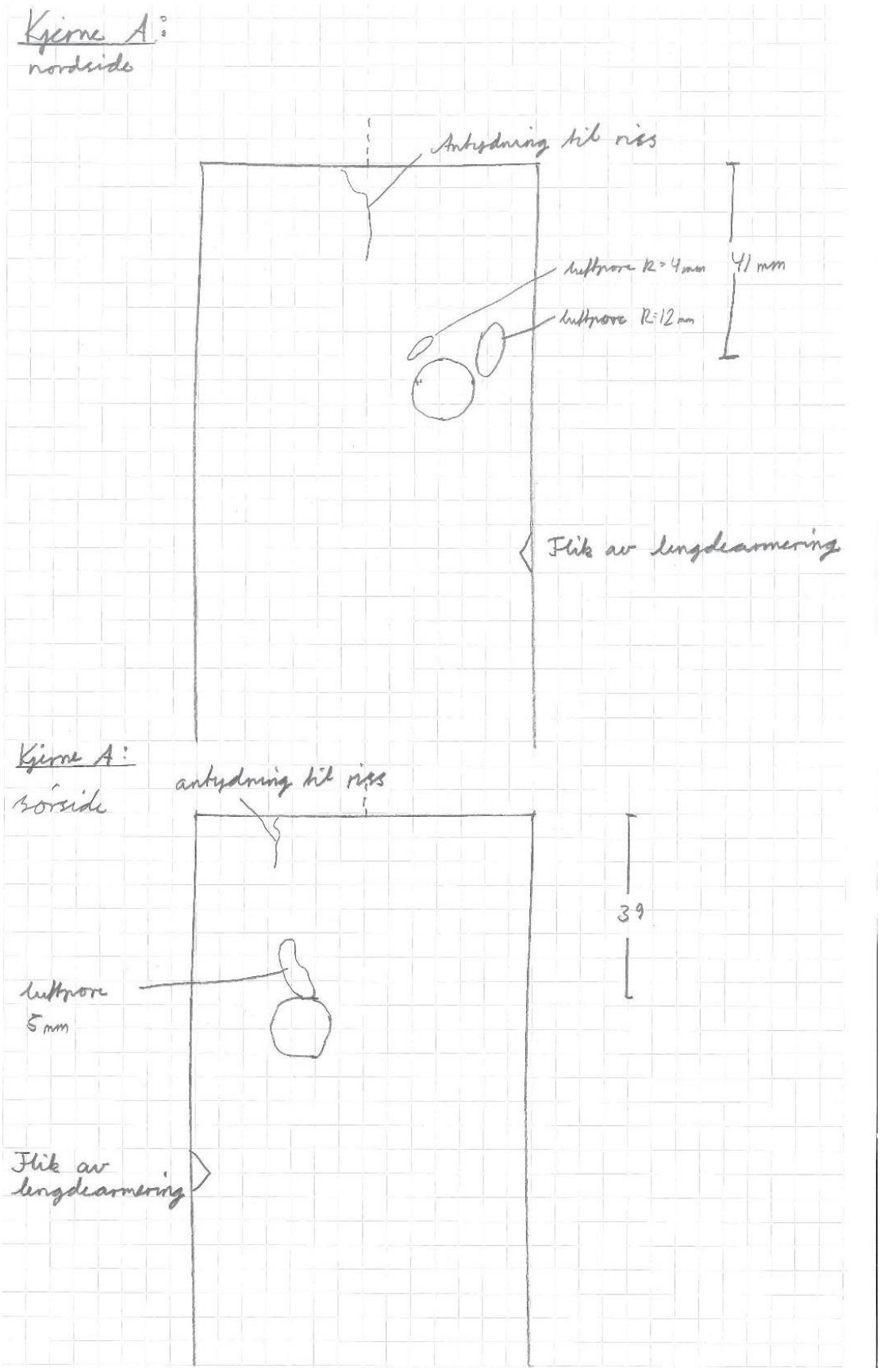

Figure 10.12 Drawing of core A with point of interest and detailed crack width.

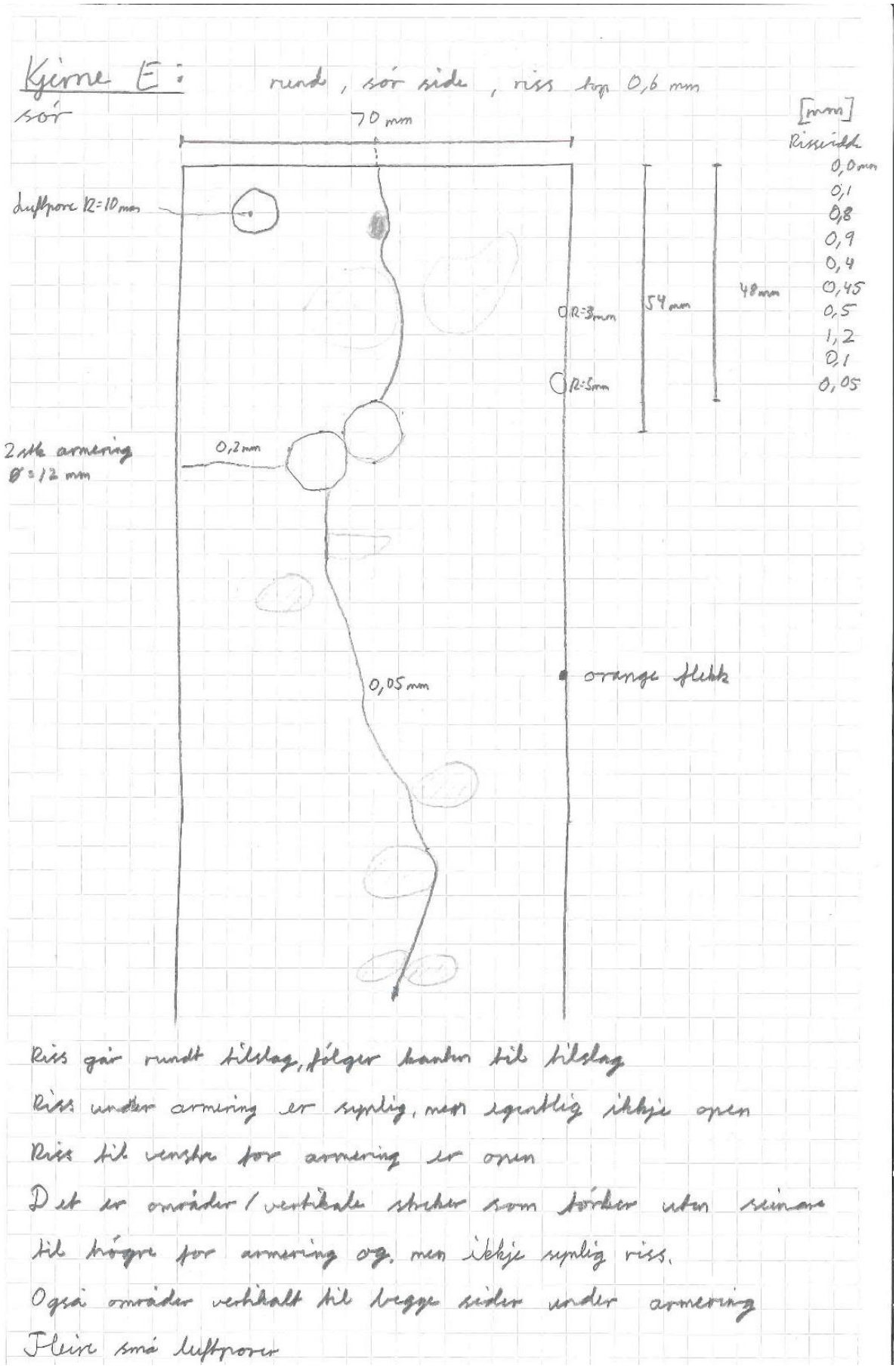

Figure 10.13 Drawing of core E, south side, with point of interest and detailed crack width.

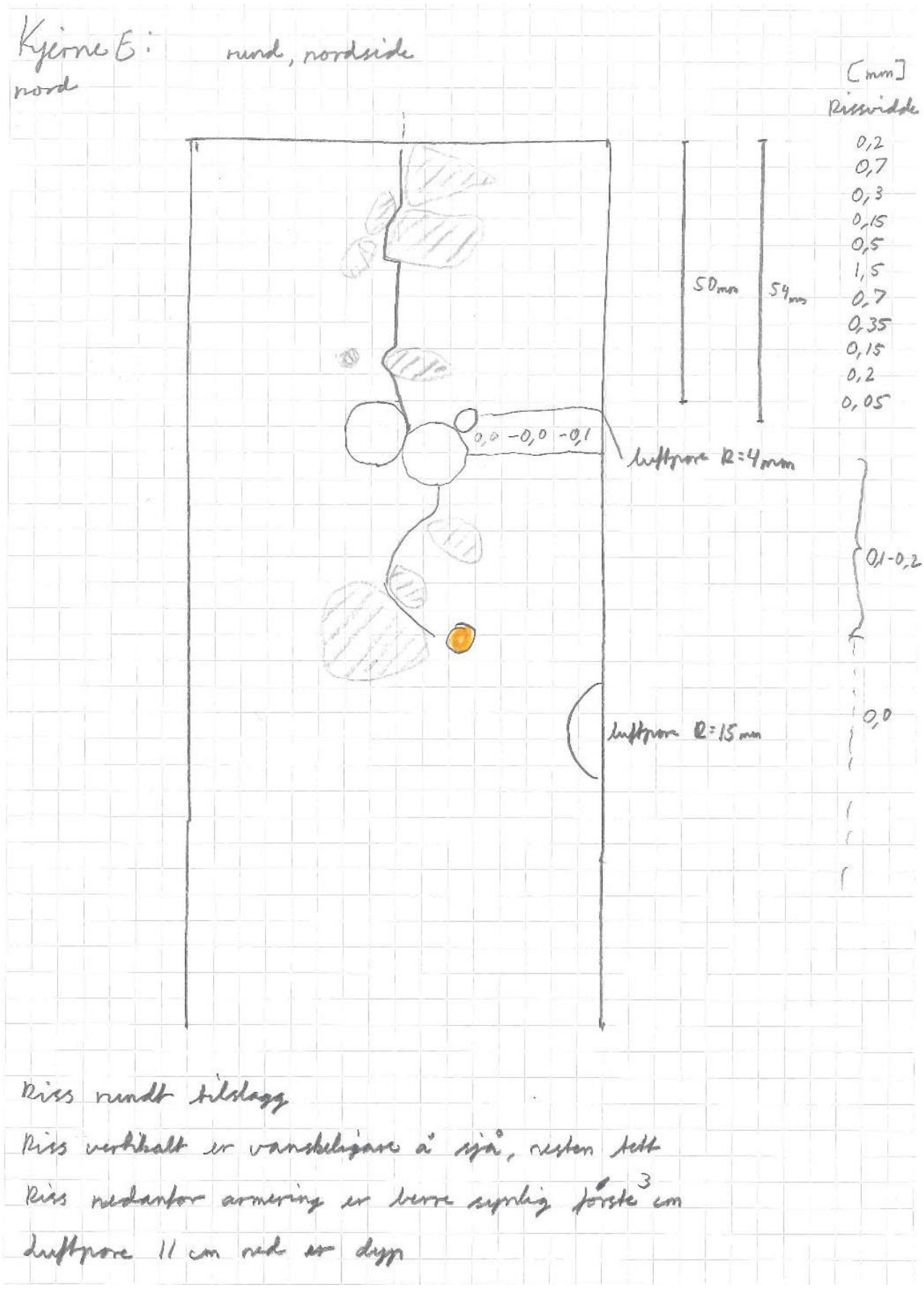

Figure 10.14 Drawing of core E, north side, with point of interest and detailed crack width.

10.6. Appendix F – Carbonation of concrete cores from Moholt- and Ceciliebridge,

Draft Note

From:	Danner, Tobias and Geiker, Mette Rica
To:	Andreas Rygg
Copy to:	Mette Geiker, Karla Hornbostel
File:	

Carbonation of concrete cores from Moholt- and Ceciliebridge

Introduction

This study is part of the ongoing research project WP7.1.1 “Relevance of crack width crack width and decompression requirements (limits) due to durability aspects of conventional reinforcement” under “Ferry free coastal route E39” initiated by the Norwegian Public Roads Administration. Within the project to Master students (Andreas Rygg and Øyvind Strømme) were contributing in spring 2017 to collect long term- field data on chloride ingress and extent of corrosion in the vicinity of cracks.

Within the Master project of Andreas Rygg at NTNU (January - June 2017) the edge beams of Moholt and Cecilie bridge in Trondheim were examined. Both bridges are exposed to de-icing salts. On both bridges, different types of cracks were observed and concrete cores were extracted at locations with and without cracks for further investigation.

In this note, measurements of carbonation depth in one core from Moholt Bridge and one core from Cecilie Bridge are described.

Concrete cores were drilled with help from Ove Loraas from the NTNU concrete laboratory. The experimental work on carbonation and extent of corrosion was undertaken by Andreas Rygg.

Structures

In Table 10.2 information about the structure, exposure and type of cracks of Cecilie and Moholt Bridge are presented. On both bridges, cracks in the edge beams were examined only. The information shown in Table 10.2 is taken from Brutus, an online bridge database maintenance by the Norwegian Public Roads Administration.

Table 10.2: Information on structure, exposure and cracks of Cecilie and Moholt bridge (BRUTUS, February 2017)

Bridge/Structure	Cecilie Bridge	Moholt Bridge
Type of structure	Beambridge	Slab bridge
Location	Trondheim, St. Olavs Hospital	Trondheim, Moholt
Year of Construction	2001	1992
Age (years)	16	25
Exposure	Deicing salt	Deicing salt
Climate	Inland	Inland
Concrete	C55, SV-40, Armering B500C	C45, m ≤ 0.4, Luft = 5 ± 1.5 %, Armering K500TS
Cover (mm)	55	50
Type and location of cracks	**Abutment:** Crack with carbonate precipitation; **Column:** Map cracking; **Edge beam:** Cracks due to shrinkage, external restraint	**Abutment:** Vertical crack in walls **Slab (Main girder):** Shear cracks **Edge beam:** Cracks due to shrinkage, external restraint, ASR

Detailed information on the structures and their exposure can be found in the Master thesis "Influence of cracks on chloride ingress and reinforcement corrosion" of Andreas Rygg (spring semester 2017).

Cores

Concrete cores were taken with a diameter of 70 mm at locations with a singular crack moving through the edge beam of the bridges. An example of the type of crack investigated is given in Figure 10.16. The concrete cores extracted from Moholt- and Ceciliebridge are shown in Figure 10.15. From now on the concrete cores will be called Core E (Moholt Bridge) and Core A (Cecilie Bridge). The investigated surface crack width was 0.55 mm and 0.45 mm at Moholt- and Cecilie Bridge respectively. The concrete core from Moholt Bridge (Core E) was taken over the stirrups in the edge beam. The cover in Core E was about 50 mm. The concrete core from Cecilie Bridge (Core A) does not contain reinforcement.

Figure 10.15: Concrete cores E and A extracted from Moholt Bridge (Left; Crack width 0.55 mm, cover 50 mm) and Cecile Bridge (right; Crack width 0.45 mm). Picture: Andreas Rygg

Figure 10.16: Investigated singular crack through the edge beam on Cecilie Bridge (Crack width 0.45 mm). Picture: Andreas Rygg

After extraction, the surface of the concrete cores was dried with paper and the cores were wrapped into plastic and stored at 5 °C. The next day the concrete cores were cut with a

water cooled concrete saw in to two halves perpendicular to the crack. The cut concrete cores were again packed into plastic and stored at 5 °C until further examination.

About two month later one half of the cores was split to extract the reinforcement in case of Moholt Bridge and to study the carbonation along the crack in both cores from Moholt- and Cecilie Bridge.

Investigation of Carbonation Depth and Extent of Corrosion

The extent of corrosion was visually investigated. Corroded rebars were cleaned in a mixture of 1:1 HCl and 3 g corrosion inhibitor (Ref to be obtained).

Carbonation depth was analysed by spraying the concrete cores with timolphtaelin indicator (Revert et al. 2016). When the surface of the concrete turns blue/violet the concrete is not carbonated. When the surface colour remains grey/brown the concrete is carbonated.

Figure 10.17 shows one half of the concrete core E from Moholt bridge. The stirrup that was located left to the crack showed uniform corrosion on the upper surface of the steel. There was also a clear imprint of corrosion products on the steel-concrete-interface facing upwards. There was no corrosion on the steel or steel-concrete-interface facing downwards to the bulk of the concrete. Corrosion was also detected on the stirrup located to the right of the crack. However, the extent of corrosion was much less.

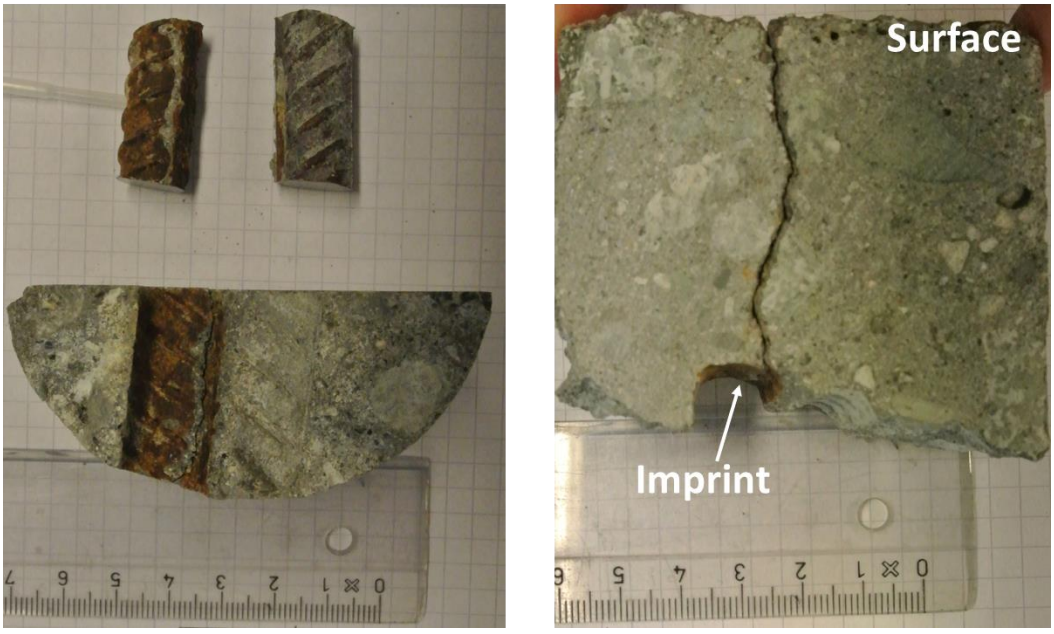

Figure 10.17: Extraction of reinforcement from the Core E from Moholt Bridge. Stirrups located left and right to the crack and imprint of corrosion products in the steel-concrete-interface facing upwards (left). Cut surface showing the crack and imprint of corrosion products in the steel-concrete-interface of the left stirrup facing upwards (right). Picture: Andreas Rygg

The extent of corrosion on the stirrup located left to the crack was also visible after cleaning with acid (Figure 10.18). The mostly corroded stirrup left to the crack and left in Figure 10.18

had a rough surface on the top part facing the exposed surface. While the stirrup to the right of the crack (right in Figure 10.18) did not have any signs of damage after cleaning with acid.

Figure 10.18: Extracted reinforcement from Core E from Moholt Bridge. Mostly Corroded stirrup located left to the crack (left), less corroded stirrup located right to the crack (right). Picture: Andreas Rygg

The carbonation depth of the exposure surface was determined to about 3 mm. To investigate the potential carbonation of the cracked surface, the concrete cores E and A were sprayed with timolphtalein indicator (Figure 10.19 and 6). The cut surfaces were uncarbonated (blue). However, the crack surfaces were completely carbonated. In addition, the imprint of the corroded part (facing the exposed surface) of the left stirrup in Core E was carbonated. The steel-concrete-interface of the left stirrup facing the bulk of the concrete and the imprint of the right stirrup were not carbonated.

A similar investigation was performed on concrete Core A from Cecilie Bridge. Core A was opened along the crack and the carbonation depth was tested on all surfaces (Figure 10.20). It can be seen that the corrosion depth on the cut surface of concrete core A is less than 1 mm. The crack surface is again completely carbonated.

Core A did not contain stirrups or reinforcement. Therefore, there is no information on the extent of corrosion available at the current time.

It was attempted to check the carbonation depth away from crack to the bulk of the concrete by splitting the concrete into smaller layers. The investigations showed that carbonation is only present at the surface of crack.

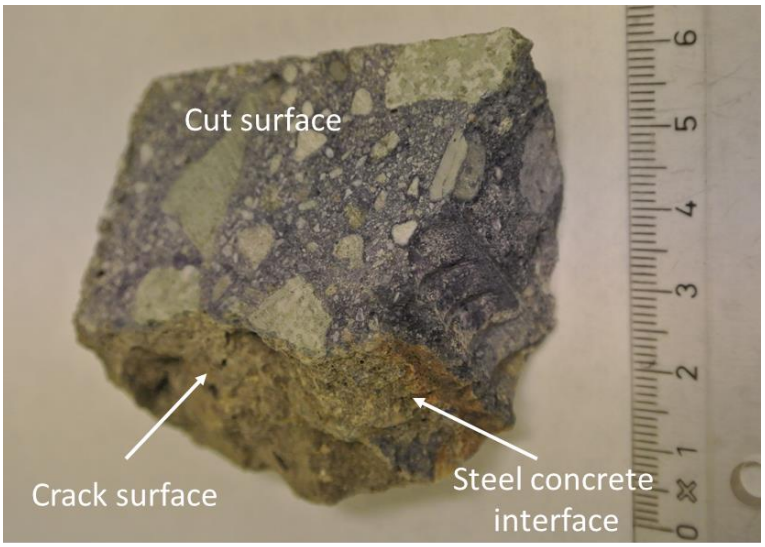

Figure 10.19: Carbonation on crack surface and cut surface of Core E from Moholt Bridge. Picture: Andreas Rygg

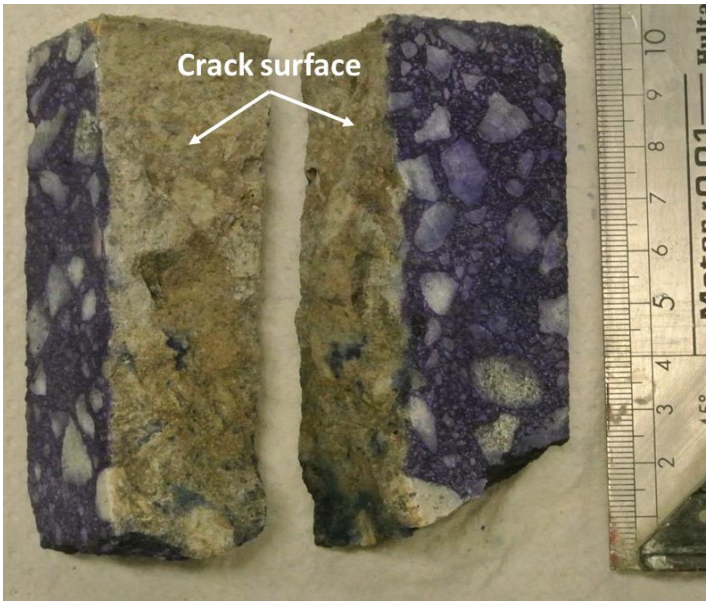

Figure 10.20: Carbonation on crack surface and cut surface of Core A from Cecilie Bridge. Picture: Andreas Rygg

Summary

Two concrete cores from the edge beams of Moholt and Cecilie Bridge were extracted at locations of cracks. The crack widths were 0.55 and 0.45 mm, respectively. The carbonation depth was investigated by spraying with a timolphtalein indicator. Crack surfaces were completely carbonated while the cut surfaces were not carbonated. In core E (from Moholt Bridge) the stirrup that was located left to the crack showed uniform corrosion on the upper surface of the steel. In addition, the imprint of the corroded part (facing the exposed surface) of the left stirrup in Core E was carbonated.

References

BRUTUS, Bruforvaltningssystem, Norwegian Public Roads Administration (NPRA), February 2017

Revert, Andres Belda; De Weerdt, Klaartje; Hornbostel, Karla; Geiker, Mette Rica. (2016) Carbonation Characterization of Mortar with Portland Cement and Fly Ash, Comparison of Techniques. Nordic Concrete Research. vol. 54 (1).